MULTILEVEL DECOMPOSITION APPROACH TO INTEGRATED AERODYNAMIC/DYNAMIC/STRUCTURAL OPTIMIZATION OF HELICOPTER ROTOR BLADES

Joanne L. Walsh

Katherine C. Young
NASA Langley Research Center
Hampton, Virginia

Jocelyn I. Pritchard
U. S. Army Vehicle Structures Directorate, ARL
Hampton, Virginia

Howard M. Adelman
NASA Langley Research Center
Hampton, Virginia

and

Wayne Mantay
U. S. Army Aeroflightdynamics Directorate, ATCOM
Hampton, Virginia

Presented at
AHS Aeromechanics Specialists Conference
Sheraton Fisherman's Wharf
San Francisco, California
January 19-21, l994

Multilevel Decomposition Approach to Integrated Aerodynamic/Dynamic/Structural Optimization of Helicopter Rotor Blades

Joanne L. Walsh and Katherine C. Young
NASA Langley Research Center

Jocelyn I. Pritchard
U. S. Army Vehicle Structures Directorate, ARL

Howard M. Adelman
NASA Langley Research Center

and

Wayne Mantay
U. S. Army Aeroflightdynamics Directorate, ATCOM
Hampton, Virginia

Abstract

This paper describes an integrated aerodynamic/dynamic/structural (IADS) optimization procedure for helicopter rotor blades. The procedure combines performance, dynamics, and structural analyses with a general purpose optimizer using multilevel decomposition techniques. At the upper level, the blade structure and response are represented in terms of global quantities (stiffnesses, mass, and average strains). At the lower level, the blade structure and response are represented in terms of local quantities (detailed dimensions and stresses).

The upper level objective function is a linear combination of performance and dynamic measures. Upper level design variables include pretwist, point of taper initiation, taper ratio, root chord, blade stiffnesses, tuning masses, and tuning mass locations. Upper level constraints consist of limits on power required in hover, forward flight, and maneuver; airfoil drag; minimum tip chord; trim; blade natural frequencies; autorotational inertia; blade weight; and average strains.

The lower level sizes the internal blade structure at several radial locations along the blade. The lower level optimization assures that a structure can be sized to provide the stiffnesses required by the upper level and assures the structural integrity of the blade. The lower level design variables are the box beam wall thicknesses and several lumped areas that are analogous to longitudinal stringers in a wing box cross section. The lower level objective function is a measure of the difference between the upper level stiffnesses and the stiffnesses computed from the wall thicknesses and lumped areas. Lower level constraints are on the Von Mises stress at the box corners for multiple load cases generated by several flight conditions, limits on wall thicknesses for thin wall theory, and other dimensional considerations.

The IADS procedure provides an optimization technique that is compatible with industrial design practices in which the aerodynamic and dynamic design is performed at a global level and the structural design is carried out at a detailed level with considerable dialogue and compromise among the aerodynamic, dynamic, and structural groups. The IADS procedure is demonstrated for several cases.

Presented at the American Helicopter Society Aeromechanics Specialists Conference, San Francisco, California, January 19-21, l994.

Notation

A	area (ft^2)
AI	autorotational inertia, $\sum_{j=1}^{ns} W_j r_j^2$ (lbm-ft^2)
a_i	ith lumped area (ft^2)
b	box width (ft)
c_d	airfoil section drag coefficient
$c_{d_{all}}$	maximum allowable section drag coefficient
$c_{d_{max}}^{\psi}$	largest section drag coefficient at azimuthal angle ψ
CF	centrifugal force (lb)
C_D	rotor coefficient of drag
C_L	rotor coefficient of lift
c_r	root chord (ft)
c_t	tip chord (ft)
DV_p	pth upper level design variable
E	Young's modulus of elasticity (lb/ft^2)
EA	extensional stiffness (lb)
EI_{xx}	chordwise bending stiffness (lb-ft^2)
EI_{zz}	flapwise bending stiffness (lb-ft^2)
f_{b_i}	ith bending frequency (per rev)

f_k	kth frequency (per rev)
f_{kl}	lower bound on kth frequency (per rev)
f_{ku}	upper bound on kth frequency (per rev)
f_{t_i}	ith torsional frequency (per rev)
F	lower level objective function
g_{c_i}	ith lower level constraint function
g_{max}	maximum lower level constraint function, $\max\{ g_{c_i} \}$
g_i	ith upper level constraint function
G	torsional modulus of elasticity (lb/ft^2)
GJ	torsional stiffness ($lb\text{-}ft^2$)
h	box height (ft)
I_{xx}	chordwise moment of inertia (ft^4)
I_{zz}	flapwise moment of inertia (ft^4)
ITER	number of trim iterations
J	polar moment of inertia (ft^4)
k_i	ith weighting factor in objective function
KS	Kresselmeir-Steinhauser function
l_f	factor of safety
m_i	ith segment tuning mass (slug/ft)
N	number of blades
n	integer
nc	number of constraints components in lower level
nP	frequency at n times rotational speed of blade
NDV	number of upper level design variables
OBJ	upper level objective function
P	main rotor power (hp)
R	blade radius from center of rotation (ft)
r	distance along blade from center of rotation (ft)
r_j	distance from center of rotation to center of jth segment (ft)
$S_{N_{ff}}$	N per rev vertical rotating hub shear in forward flight (lbf)
$S_{N_{ref}}$	reference N per rev rotating vertical hub shear in forward flight (lbf)
t_k	kth wall thickness (ft)
v_i	ith lower level design variable
$V(\sigma,\tau)$	Von Mises stress (lb/ft^2)
W	total blade weight (lbm)
W_j	total weight of jth structural segment (lbm)
y_i	location of ith tuning mass
y_{tr}	point of taper initiation
Δf	increment used in frequency window (per rev)
ε	coordination parameter
ε_y	average strain
λ	Lagrange multiplier
ρ	pull down factor
σ	bending stress (lb/ft^2)
τ	shear stress (lb/ft^2)
Ψ	azimuth angle, zero over tail (deg)
θ_{tw}	maximum pretwist (deg)

Subscripts

a	available or allowable
ff	forward flight
h	hover
m	maneuver
max	maximum
min	minimum
ref	reference

Superscripts

L	lower level
U	upper level
—	nondimensional

Introduction

Over the last decade optimization techniques have been studied for application to the rotor blade design process. In Ref. 1 Miura presents a survey on the application of numerical optimization methods to helicopter design problems including rotor blade design. Most optimization procedures have dealt with a single discipline such as aerodynamics (Refs. 2-4), structures (Ref. 5), or dynamics (Refs. 2, 6-9). However, the rotor blade design process is multidisciplinary involving couplings and interactions between several disciplines such as aerodynamics, dynamics, structures, and acoustics. These couplings and interactions can be exploited by the optimization procedure if all the disciplines are accounted for simultaneously rather than sequentially. For instance, in a review (Ref. 10) on the impact of structural optimization on vibration reduction, Friedmann emphasizes the need to include the multidisciplinary couplings between aerodynamics, dynamics, and structures even when optimizing only for minimum vibration.

Techniques and strategies for merging disciplines to obtain integrated rotorcraft optimization procedures are developing. In Refs. 11 and 12, a plan is described for integrating the disciplines of aerodynamics, dynamics, structures, and acoustics. As part of that plan, aerodynamics and dynamics have been incorporated systematically into performance (Refs. 3 and 4) and airload/dynamic (Ref. 13) optimization procedures resulting in an integrated aerodynamic/dynamic optimization procedure (Ref. 14). Ref. 15 summarizes recent accomplishments based on that plan.

Other multidisciplinary rotor blade optimization work is described in Refs. 16-19. Refs. 16 and 17 describe the formulation of a multidisciplinary approach to rotor blade design for improved performance and reduced fuselage vibrations. Ref. 18 describes a staged optimization procedure for a rotor for combined aerodynamics, dynamics, and structures. Ref. 19 describes a multidisciplinary optimization procedure to design high speed prop rotors.

What is lacking in previous multidisciplinary rotor blade optimization procedures is an efficient method to integrate structures or structural properties. Usually structures or structural properties are included in one of two ways - either as local design variables (indirectly affecting the response of the blade) or global design variables (directly affecting the response of the blade). When local design variables are used, the detail dimensions of a structural member at one or more radial locations along the blade are used to generate structural properties. When global design variables are used, structural properties are the design variables. Both type of design variables have limitations. Using local design variables (e.g., Refs. 6,7,18-19), such as wall thicknesses of the structural member, can lead to a large number of design variables which can be computationally expensive. Also, this choice of design variables is at odds with traditional design practice where chord, stiffness, and mass distributions along the blade are determined and then a structure is designed which matches these distributions. Using global design variables (e.g., Refs. 2,9,13,14,16-17), such as stiffness and mass properties, in optimization also has disadvantages. When flapwise bending stiffness, chordwise bending stiffness, torsional stiffness, and extensional stiffness distributions are used as design variables, they are treated as independent quantities. In reality, these stiffnesses are not independent, and there is no guarantee that a set of wall thicknesses can be found which will simultaneously give these stiffnesses.

This paper presents the methodology for incorporating aerodynamics, dynamics, and structures in an integrated optimization procedure using both local and global design variables. Multilevel decomposition techniques based on Ref. 20 are used to add structural design variables and constraints to an existing aerodynamic/dynamic optimization procedure (Ref. 14). The product is an integrated aerodynamic/dynamic/structural optimization (IADS) procedure. The multilevel decomposition formulation used in this paper was presented first in Ref. 15. Another preliminary study of multilevel decomposition techniques applied to rotor blade design is described in Ref. 21.

The multilevel decomposition approach has been successfully applied to multidisciplinary problems (e.g., Refs. 22-24). As originally proposed in Ref. 25, the coordination procedure consisted of an optimum sensitivity analysis (Ref. 26) and a set of equality constraints which relate the detailed (local) design variables of one subsystem to the global design variables on the level above. However, as pointed out in Ref. 27, these equality constraints have caused difficulties in implementing multilevel decomposition procedures. The IADS procedure is based on the multilevel decomposition approach of Ref. 20 which eliminates the equality constraints in the coordination procedure allowing the use of the less computationally costly optimum sensitivity derivative found in Ref. 28. However in the IADS procedure, the set of lower level constraints is replaced by an envelope function known as the Kresselmeir-Steinhauser function (KS-function, Ref. 29) which further reduces computational cost.

First, the general multilevel decomposition strategy with two levels will be discussed (note: systems with more levels are discussed in Refs. 20, 22, and 25). Next, the general strategy will be related to rotor blade design. Then, the IADS development including flowcharts of the upper and lower levels and the optimization procedure will be explained. Results will be presented for several cases which demonstrate the strengths of the IADS procedure.

Multilevel Decomposition Optimization Strategy

With a multilevel decomposition approach (Refs. 20, 22, and 25), a large complex optimization problem is broken into a hierarchy of smaller optimization subproblems. This hierarchy can be thought of as levels of increasing detail. At the upper level, the subproblem is formulated in terms of global quantities which describe the overall behavior of the entire system. On the lower level, the subproblems are stated in terms of local quantities and local constraints which have only a small impact on the entire system. Each subproblem uses local design variables to reduce the violation of constraints which are unique to that subproblem. The coupling between the upper level subproblem and the lower level subproblems is preserved through a coordination procedure such as that described in Refs. 20 or 25. This coupling represents a dialogue between the levels that upon convergence establishes compatibility between the two levels.

Fig. 1 illustrates a generic two-level optimization procedure. Note that the analysis proceeds from the upper level to the lower level while the optimization proceeds from the lower level to the upper level. First, the upper level analysis initializes all the global quantities and responses and then provides information to each lower level subproblem. Individual lower level optimizations are performed which reduce local constraint violations as much as possible and which provides information to the coordination procedure. Next the upper level optimization occurs. The preceding describes one cycle. The entire process is repeated for several cycles. Convergence occurs when all the constraints (both upper level and lower level) are satisfied and the upper level objective function is minimized.

The rotor blade optimization problem can be decomposed into one subproblem affecting the global response of the blade and three subproblems affecting portions of the blade. Quantities such as power required, blade trim, autorotational inertia, natural frequencies, total blade weight, and average strain describe the global response of the blade. The entire blade must be analyzed to obtain these response quantities. Quantities such as stresses are detailed response quantities since only a portion of the blade must

be analyzed to obtain these response quantities. Therefore, a two-level decomposed rotor blade optimization problem can be defined as shown in Fig. 2. The upper level optimizes the blade by changing global quantities such as blade planform, twist, and distributions of mass and stiffness. The upper level chord, mass, and stiffness distributions are treated as independent quantities. The reconciliation between these distributions is done on the lower level. The lower level consists of several independent subproblems at stations along the blade radius, which optimize detailed cross-sectional dimensions to satisfy stress constraints and reconcile the upper level independent mass, chord, and stiffness distributions with the lower level calculated stiffness distributions. This reconciliation is improved further by a set of upper level coordination constraints (see Appendix A). First the upper level analysis and optimization will be described, then the lower level analysis and optimization, and then the overall IADS system.

Upper Level Analysis and Optimization

The purpose of the upper level analysis is to evaluate the overall rotor blade design on the basis of performance, dynamic, and global structural measures. (For a description of the rotor blade design philosophy see Refs. 3-4, 11-12, and 14-15.) The upper level analysis is similar to the integrated aerodynamic/dynamic analysis reported in Ref. 14 with the addition of extensional stiffness design variables, strain constraints, and coordination constraints. As shown in Fig. 3, the blade is analyzed for three flight conditions: hover, forward flight, and maneuver. The Langley-developed hover analysis program HOVT (a blade element momentum analysis based on Ref. 30) is used to predict power required in hover. The comprehensive helicopter analysis program CAMRAD/JA (Ref. 31) is used to predict rotor performance (e.g., trim, airfoil drag, power required), loads, and frequencies for forward flight and maneuver. The maneuver flight condition simulates a coordinated turn in terms of a increased load on the forward flight lift requirement.

Upper Level Design Variables - The upper level design variables are the blade planform, stiffnesses, and tuning masses (see Fig. 4). The blade planform is defined by the point of taper initiation y_{tr}, root chord c_r, taper ratio c_r/c_t, and maximum pretwist θ_{tw}. The blade is rectangular from the root to y_{tr} and then tapers linearly to the tip. The pretwist varies linearly from the center of rotation to the tip. Global design variables include the blade chordwise, flapwise, torsional, and extensional stiffnesses (denoted by EI_{xx}, EI_{zz}, GJ, and EA, respectively) at three radial locations: blade root, point of taper initiation, and blade tip. The stiffnesses are assumed to vary linearly between these points and are treated as independent quantities. The remaining design variables are three tuning masses (denoted by m_1, m_2, m_3) and their locations (denoted by y_1, y_2, and y_3). The total blade mass consists of the structural mass (which is assumed constant) plus the sum of the tuning masses. There is no attempt to reconcile the change in weight with the change in design variables since the present work is based on extending the procedure of Ref. 14 to include structures. However, this reconciliation is possible (see Ref. 15). It is assumed that the center of gravity and aerodynamic offsets are coincident with the blade elastic axis. The number of blades, rotor radius, rotational velocity, airfoils, and airfoil distribution are preselected and fixed.

Upper Level Objective function - The objective function to be minimized is a combination of performance and dynamics measures and is formulated as follows

$$OBJ = k_1 \frac{P_h}{P_{h_{ref}}} + k_2 \frac{P_{ff}}{P_{ff_{ref}}} + k_3 \frac{P_m}{P_{m_{ref}}} + k_4 \frac{S_{N_{ff}}}{S_{N_{ref}}} \qquad (1)$$

where P_h, P_{ff}, and P_m are the powers required in hover, forward flight, and maneuver, respectively. N is the number of blades and $S_{N_{ff}}$ is the N per rev rotating vertical hub shear in forward flight. The terms k_1, k_2, k_3, and k_4 are weighting factors chosen by the user. $P_{h_{ref}}$, $P_{ff_{ref}}$, $P_{m_{ref}}$, and $S_{N_{ref}}$ are reference values used to normalize and nondimensionalize the objective function components. The usefulness of this objective function was demonstrated in Ref. 14.

Upper Level Constraints - The rotor blade design process is defined in terms of aerodynamic performance, dynamics, and global structural requirements. Satisfactory aerodynamic performance is defined by the following four requirements. First, the power required for any flight condition must be less than the available power. Second, airfoil section drag along the blade radius on the advancing and retreating side of the rotor disk in both forward flight and maneuver must be less than a maximum allowable value. Third, the rotor must trim at each flight condition. The rotor is trimmed to a constant lift in forward flight and a (different) constant lift in maneuver which ensures that the rotor has no loss in lift capability or maneuverability even if solidity decreases from the initial to the final design. Incorporation of a maneuver flight condition is used in place of a constraint on solidity, since low speed maneuver determines rotor solidity (Ref. 32). Fourth, the blade tip chord must be larger than a prescribed minimum value. Satisfactory dynamics is defined in terms of limits on vibrational frequencies. The blade is designed so that the natural frequencies (both bending and torsional) do not coincide with integer multiples of the rotor speed. Also, the blade must have sufficient autorotational inertia as a safety measure needed in case of engine failure. In addition to satisfying these design requirements, the blade

weight must not exceed some upper limit. Satisfactory structural requirements are defined in terms of limits on the average axial strains for forward flight and the maneuver flight conditions.

This section of the paper discusses the performance, dynamic, and structural constraints. The coordination constraints are discussed later in the paper. The performance and dynamic constraints are the same as those used in Ref. 14. By convention, the ith constraint g_i is satisfied if it is less than or equal to zero.

Performance Constraints - The performance constraints are on power required, trim, airfoil section drag, and blade tip chord. The requirement that the power required be less than the power available is given by

$$g_i = \frac{P_j}{P_a} - 1 \le 0 \qquad \text{for each flight condition} \qquad (2)$$

where P_j is the power required for the ith flight condition and P_a is the power available.

The requirement on the airfoil section drag translates into a constraint that each airfoil section distributed along the rotor blade operate at a section drag coefficient c_d less than a specified allowable value $c_{d_{all}}$ (see Ref. 14). This leads to 24 constraints per flight condition since the blade is analyzed in 15 degree azimuthal increments around the rotor disk. At a given azimuthal angle Ψ the constraint is formulated as

$$g_i = \frac{c_{d_{max}}^{\Psi}}{c_{d_{all}}} - 1 \le 0 \qquad \Psi=15,\ 30,\ 45,...,\ 360 \qquad (3)$$

where $c_{d_{all}}$ is the allowable drag coefficient and $c_{d_{max}}^{\Psi}$ is the largest drag coefficient at any radial station (note: the drag coefficients in the reverse flow region occurring on the retreating side of the rotor disc are ignored). In the present work the same value for $c_{d_{all}}$ is used on the advancing and retreating side of the rotor disk. This simplifying assumption could easily be lifted.

The trim requirement is difficult to translate into a mathematical constraint. The trim constraints in forward flight and maneuver are implemented using the method developed in Ref. 3 which expresses the constraint in terms of the number of trim iterations (ITER), the maximum number of trim iterations allowed ($ITER_{max}$), and the pth nondimensional design variable ($\overline{DV}_p$). The heuristic trim constraint is given by

$$g_i = (ITER - ITER_{max} + 1)\left(\sum_{p=1}^{NDV} \overline{DV}_p\right) \le 0 \qquad (4)$$

where NDV is the number of design variables. In development of this equation in Ref. 3, it was found that the addition of the summation term improved convergence because it allowed calculation of the change in the trim constraint with respect to change in a single design variable.

The final performance requirement is a constraint used to ensure that the blade tip chord does not become too small

$$g_i = 1 - \frac{c_t}{c_{t_{min}}} \le 0 \qquad (5)$$

where c_t is the tip chord and $c_{t_{min}}$ is the minimum tip chord allowed. This is a practical constraint used to assure validity of the airfoil tables and address manufacturing considerations.

Dynamic Constraints - The dynamic constraints are on frequencies, total blade weight, and autorotational inertia. The constraint on the kth frequency f_k (either a bending or a torsional frequency) is formulated such that the frequency is separated from integer multiples of the rotor speed by an amount Δf

$$g_i = \frac{f_k}{f_{ku}} - 1 \le 0 \qquad \text{(upper bound)} \qquad (6a)$$

and

$$g_i = 1 - \frac{f_k}{f_{kl}} \le 0 \qquad \text{(lower bound)} \qquad (6b)$$

where f_{ku} has a value that is Δf below n+1 per rev and f_{kl} has a value that is Δf above n per rev for the applicable n. For example, suppose Δf is 0.1 per rev and f_4 is 5.6 per rev, then nP would be 5 per rev and (n+1)P would be 6 per rev. Thus f_{4u} and f_{4l} would be 5.9 per rev and 5.1 per rev, respectively. Formulating the constraints in this manner allows the frequencies to change from one optimization cycle to the next cycle provided the frequencies avoid approaching integer multiples of the rotor speed. This formulation is different from the approaches used in Refs. 13 and 16-17 where the frequencies are kept within prescribed windows based on the reference blade frequencies. In this work, constraints are placed on frequencies in both forward flight and maneuver since blade collective pitch and the amount of modal coupling may be different for the two flight conditions and therefore the frequencies could be different.

The constraint that the blade weight be less than some maximum value is formulated as follows

$$g_i = \frac{W}{W_{max}} - 1 \le 0 \tag{7}$$

where W is the total blade weight and W_{max} is the maximum allowable weight. The total blade weight is the structural mass distribution (which is constant) plus the sum of the tuning masses.

Finally, the blade must have enough autorotational inertia AI for safe autorotation in case of engine failure. The constraint is formulated so that the autorotational inertia of the blade is greater than some minimum value AI_{min}

$$g_i = 1 - \frac{AI}{AI_{min}} \le 0 \tag{8}$$

Structural Constraints - The structural constraints are on the average axial strains. The structural constraints which are evaluated at the same radial locations used to define the design variables (Fig. 4) are imposed on the average axial strains ε_y as follows

$$g_i = \frac{\varepsilon_y}{\varepsilon_a} - 1 \le 0 \tag{9a}$$

and

$$g_i = -1 - \frac{\varepsilon_y}{\varepsilon_a} \le 0 \tag{9b}$$

where ε_a is the magnitude of the allowable strain and

$$\varepsilon_y = \frac{l_f CF}{EA} \tag{10}$$

where CF is the centrifugal force, EA is the extensional stiffness, and l_f is a safety factor on the loads. The strain constraints are calculated using loads from both the forward flight and the maneuver flight conditions.

Upper Level Optimization - The upper level optimization consists of the general purpose optimization program CONMIN (Ref. 33) and an approximate analysis used to reduce the number of HOVT and CAMRAD/JA analyses during the iteration process. The approximate analysis is used to extrapolate the upper level objective function and upper level constraints with linear Taylor Series expansions using derivatives of the objective function and constraints with respect to the design variables

$$OBJ = OBJ_0 + \sum_{i=1}^{NDV} \left.\frac{\partial OBJ}{\partial DV_i}\right|_0 \Delta DV_i \tag{11}$$

$$g = g_0 + \sum_{i=1}^{NDV} \left.\frac{\partial g}{\partial DV_i}\right|_0 \Delta DV_i \tag{12}$$

The assumption of linearity is valid over a suitably small change in the design variable values and will not introduce a large error into the analysis provided the changes ΔDV_i are small. Errors which may be introduced by use of the approximate analysis are controlled by imposing "move limits" on each design variable during the iteration process. A move limit which is specified as a fractional change of each design variable value is imposed as an upper and lower design variable bound. At the present time the move limits are manually adjusted.

Lower Level Analysis and Optimization

This section of the paper describes the lower level analysis and lower level optimization procedure. The purpose of each lower level optimization is to assess whether a structure at the given radial location can be sized to provide the stiffnesses required by the upper level optimization and have the strength to withstand loads calculated by the upper level analysis. The lower level optimizations can be done in parallel since they are independent.

For simplicity, since closed-form equations can be derived (see Appendix B), the structural member (Fig. 5) is assumed to be a thin-walled isotropic box. The box cross section is symmetric about the horizontal axis with wall thicknesses t_i and lumped areas a_j which are analogous to longitudinal stringers in a wing box cross section. The outer dimensions b (the box beam width) and h (the box beam height) are functions of the upper level design variables since b and h depend on the local chord and the local airfoil thickness. The values of b and h are determined by placing a box of maximum area within the airfoil cross section using the method of Ref. 34.

Lower Level Design Variables - The design variables are the three wall thicknesses (t_1, t_2, and t_4) and the three lumped areas (a_1, a_2, and a_3). The lumped areas are used to give the lower level more flexibility in matching the upper level stiffnesses. For the present implementation, the lumped areas are assumed to be square areas.

Lower Level Objective Function - The objective function is a measure of the difference between the stiffnesses required on the upper level and those determined from the lower design variables

$$F = \left(\frac{\left(EI_{zz} - (EI_{zz})^*\right)}{(EI_{zz})^*}\right)^2 + \left(\frac{\left(EI_{xx} - (EI_{xx})^*\right)}{(EI_{xx})^*}\right)^2 + \left(\frac{\left(GJ - (GJ)^*\right)}{(GJ)^*}\right)^2 \tag{13}$$

where a starred quantity ( )* denotes an upper level design variable. The lower level cross sectional properties I_{xx}, I_{zz}, and J are computed (see Appendix B), E is Young's modulus of elasticity, and G is the torsional modulus of elasticity.

Lower Level Constraints - The constraints are enforced on the extensional stiffness, stresses, and the physical dimensions of the wall thicknesses and lumped areas. The extensional stiffness constraint which requires the lower level calculated extensional stiffness EA (see Appendix B) to be equal or greater than the upper level extensional stiffness $(EA)^*$ (an upper level design variable) is given by

$$g_{c_i} = 1 - \frac{EA}{(EA)^*} \le 0 \tag{14}$$

at the given cross section. It is noted that the extensional stiffnesses appear in a constraint rather than in the objective function (Eq. 13) where the other stiffnesses appear. This is done for the following reason. The role of EA in the upper level is limited to satisfying the strain constraints (Eq. 9). The lower level is responsible only for assuring that the value of EA is at least as large as the value needed in the upper level -- close matching of EA to $(EA)^*$ is not required.

The stress constraint which is evaluated at the corner of the box cross section shown in Fig. 5 has the following form

$$g_{c_i} = \frac{V(\sigma,\tau)}{\sigma_a} - 1 \le 0 \tag{15}$$

where σ is the bending stress, τ is the shear stress, and $V(\sigma,\tau)$ is the Von Mises stress measure (see Appendix B). Two stress constraints are used - in one τ is based on the vertical wall thickness and in the other τ is based on the horizontal wall thickness.

A set of constraints is imposed on the lower level wall thicknesses to assures that the section remains a thin-walled section and that the expression for J remains valid (see Appendix B). These constraints are

$$g_{c_i} = \frac{t_j}{0.1b} - 1 \le 0 \qquad j = 2 \text{ and } 4 \tag{16}$$

$$g_{c_i} = \frac{t_j}{0.1h} - 1 \le 0 \qquad j = 1 \text{ and } 3 \tag{17}$$

where b and h are the width and height of the box cross section, respectively.

A set of constraints is imposed on the lumped areas and wall thicknesses which require that the dimensions are physically possible (i.e. the lumped areas can fit inside of the box cross section. These constraints are

$$g_{c_i} = -\left[\frac{b - t_4 - t_2}{2} - \sqrt{a_1} - \frac{1}{2}\sqrt{a_2}\right] \le 0 \tag{18}$$

$$g_{c_i} = -\left[\frac{b - t_4 - t_2}{2} - \sqrt{a_3} - \frac{1}{2}\sqrt{a_2}\right] \le 0 \tag{19}$$

$$g_{c_i} = -\left[h - t_1 - t_3 - 2\sqrt{a_1}\right] \le 0 \tag{20}$$

$$g_{c_i} = -\left[h - t_1 - t_3 - 2\sqrt{a_2}\right] \le 0 \tag{21}$$

$$g_{c_i} = -\left[h - t_1 - t_3 - 2\sqrt{a_3}\right] \le 0 \tag{22}$$

In addition a set of constraints representing upper and lower bounds on the design variables is used. For the kth design variable, the lower bound is given by

$$g_{c_i} = v_{k_l} - v_k \le 0 \tag{23}$$

and the upper bound by

$$g_{c_i} = v_k - v_{k_u} \le 0 \tag{24}$$

where v_{k_l} and v_{k_u} are the lower and upper design variable bound, respectively.

For convenience, the set of lower level constraints defined by Eqs.14-24 is replaced by a single cumulative constraint, an envelope function known as the KS function (Ref. 29), which approximates the active constraint boundary

$$KS = g_{max} + \frac{1}{\rho}\ln\left[\sum_{j=1}^{nc} e^{\rho(g_{c_j} - g_{max})}\right] \le 0 \tag{25}$$

where g_{max} is the maximum constraint component from Eqs.14-24, nc is the number of lower level constraint components and ρ is defined by the user. Initially ρ is small and then increases until a maximum value ρ_{max} is reached. For large values of ρ, the value of KS approaches g_{max}. The KS function is a single measure of the degree of constraint satisfaction or violation and is positive (violated) if at least one of the constraints g_{c_i} is violated. The KS function is a single-valued function which is continuous and differentiable. This property becomes important when implementing the upper and lower levels as described in

the section on the overall organization of the IADS procedure.

Lower Level Optimization Procedure - The flowchart for each lower level optimization procedure is shown in Fig. 6. Loads, local chord, box beam width, box beam height, and upper level stiffnesses are passed down from the upper level analysis. The lower level design variables (Fig. 5) are used to calculate lower level stiffnesses. Von Mises stresses are calculated using the loads from the forward flight and maneuver analyses. The lower level objective function (Eq. 13) and cumulative constraint (Eq. 25) are evaluated. The lower level optimizations are performed using the general purpose optimization program CONMIN. Exact analyses are used to evaluate the objective function, the constraint, and any gradients computed by CONMIN. The optimization process is converged when the objective function is minimized and the cumulative constraint is satisfied. After convergence the process returns to the upper level.

Coordination Between Upper and Lower Levels

The coordination between upper and lower levels is implemented by upper level constraints. These constraints are imposed to encourage changes in the upper level design variables which promote consistency between the upper and lower level stiffnesses. Specifically, these constraints (one for each lower level optimization) have the form

$$g = F^U - (1+\varepsilon)F_o^L \le 0 \tag{26}$$

where F_o^L is the most recent value of the lower level objective function (i.e., optimum value of Eq. 13), F^U is an estimate of the change in F_o^L which would be caused by a change in the upper level design variable values, and ε is a specified tolerance denoted the coordination parameter (see Appendix A). The importance of this parameter will be discussed later.

Eq. 26 is the general form of the coordination constraint as formulated in Ref. 15. As shown in Appendix A, the coordination constraint can be approximated in terms of the lower level total optimum sensitivity derivative which expresses how the optimum lower level objective function and lower level active constraint will change with a change in upper level design variable.

Overall Organization of IADS Procedure

The conceptual IADS procedure is shown in Fig. 2. It consists of an upper level analysis (Fig. 3), three lower level optimizations (Fig. 6), and a coordination task. The actual IADS procedure is more complicated and requires an upper level sensitivity analysis and three lower level optimum sensitivity analyses in addition.

The flowchart for the IADS procedure is shown in Fig. 7. First, the upper level analysis is executed for the current set of design variables providing all of the information needed to calculate the upper level objective function and constraints with the exception of the coordination constraints. The upper level analysis also provides the loads, local chord, box beam width, box beam height, and stiffnesses (to be matched) to the lower level analysis. Each lower level optimization is performed to obtain a set of lower level design variables which match the current upper level bending and torsional stiffnesses as close as possible.

Next, an upper level sensitivity analysis is performed consisting of forward finite difference derivatives (or gradients) of the upper level analysis. These derivatives of the upper level objective function and upper level constraints are required to approximate the upper level objective function and upper level constraints during the upper level optimization. In addition, the loads and local chords corresponding to the changes in the upper design variables are saved. These quantities are used in the three lower level optimum sensitivity analyses to approximate the coordination constraint (Eq. 26). Appendix A describes how the coordination constraint is expressed in terms of the total optimum sensitivity derivative involving changes in the optimum lower level objective function with respect to changes in the upper level design variables and changes in the active lower level constraint with respect to changes in the upper level design variables.

Finally, the upper level optimization consisting of CONMIN and approximate analysis occurs. This describes one cycle of the IADS procedure. The process is repeated for additional cycles until convergence is achieved. A very strict convergence criterion is used for demonstration purposes. The overall procedure is converged when the change in the upper level objective function is less than 0.5×10^{-5} over three consecutive cycles and all the constraints (both upper and lower level) are satisfied. A step size of 0.001 is used to compute the finite difference derivatives.

Demonstration of the IADS Procedure

This section of the paper describes the analytical blade model, the mission definition, the optimization problem, and optimization results used to demonstrate the IADS procedure. Results are presented for two studies - (1) the effect of initial design and (2) the effect of the coordination parameter ε.

Analytical Blade Model - The analytical blade model used to demonstrate the IADS procedure represents a wind

tunnel model of a rotor blade for a four-bladed helicopter. The blade has radius is 4.68 ft. Three sets of advanced airfoils are used along the blade - the RC(4)-10 airfoil (Ref. 35) from the root to 85 percent radius, the RC(3)-10 (Ref. 36) airfoil from 85 to 95 percent radius, and the RC(3)-08 (Ref. 36) airfoil from 95 percent radius to the tip. Tables of experimental two-dimensional airfoil data for these three airfoil types are used in both HOVT and CAMRAD/JA. The analytical model of the blade uses 19 aerodynamic segments for HOVT, 50 structural segments and 18 aerodynamic segments for CAMRAD/JA. HOVT is used to predict the power required in hover using nonuniform inflow (no wake is included) by trimming to a constant lift C_L. CAMRAD/JA is used to predict rotor performance, loads, and frequencies using uniform inflow with empirical inflow correction factors for the forward flight and maneuver flight conditions. Uniform inflow is used to save on computational costs (note: even though approximate analysis is used in the upper level optimization 46 CAMRAD/JA analyses are required per optimization cycle). In CAMRAD/JA an isolated rotor analysis is used which trims the rotor to constant lift C_L and drag C_D and zero flapping angle relative to the shaft using collective, lateral cyclic, and longitudinal cyclic pitch. From the modal analyses in CAMRAD/JA using ten bending modes and five torsional modes, it is found that only the first six bending frequencies are below 10 per rev and need to be constrained for a four-bladed rotor. Since f_{b_1} corresponds to a rigid body mode and f_{b_2} is the 1 per rev, the first two frequencies are not constrained. Constraints are placed on the first four bending frequencies (f_{b_3}, f_{b_4}, and f_{b_6} flapping-dominated and f_{b_5} lead-lag dominated) and the first two torsional frequencies (f_{t_1} representing the rigid body torsional mode due to the control system stiffness and f_{t_2} representing the first elastic torsional mode).

Mission Definition - The flight conditions are a constant lift of 1-g (331 pounds, C_L=0.0081), propulsive force of 32 pounds (C_D=-0.000811), and an advance ratio of 0.35 for the forward flight condition and a constant lift of 401 pounds (C_L=0.00985), a propulsive force of 23 pounds (C_D=-0.000596), and an advance ratio of 0.3 for the maneuver flight condition. The maneuver flight condition is for a load factor of 1.22. These flight conditions and load factor are similar to those used in Ref. 37.

Optimization problem - The objective function is a combination of the power required in hover, forward flight, and maneuver and the 4 per rev rotating vertical hub shear in forward flight. The objective function is chosen to be one dominated by performance with little emphasis on dynamics. Of the three powers it is assumed that it is most important to reduce the power required in hover - it will have twice the weight as the other two powers. Several values were tried for the weighting factor on the hub shear term. It was found that to obtain the proper balance between performance and dynamics, k_4 has to be between one and two orders of magnitude less than k_1. Thus, for this case, the weighting factors are chosen to be k_1 =10.0, k_2=k_3=5.0, and k_4 = 0.5.

$$OBJ = 10\frac{P_h}{P_{h_{ref}}} + 5\frac{P_{ff}}{P_{ff_{ref}}} + 5\frac{P_m}{P_{m_{ref}}} + 0.5\frac{S_{4_{ff}}}{S_{4_{ref}}} \qquad (30)$$

where $P_{h_{ref}}$, $P_{ff_{ref}}$, $P_{m_{ref}}$, and $S_{4_{ref}}$ are 15 hp, 13 hp, 12 hp, and 2 lbf, respectively. The reference values are chosen to be representative of the powers required and hub shear for all the initial blade designs used in this work.

The upper and lower bounds for the design variables are given in Table 1. On the upper level twenty-two design variables and 95 constraints are used. On the lower level six design variables and one cumulative constraint (the KS-function with 24 components) are used at each of the three spanwise locations (i.e., the root, the point of taper initiation, and the tip).

Parameters and flight conditions are summarized in Table 2. Since the blade is made of aluminum, E has a value of 15.26×10^8 lb/ft^2, the allowable strain ε_a has a value of 0.05 ft/ft, and the allowable stress σ_a is 8.352×10^6 lb/ft^2. The values for minimum tip chord $c_{t_{min}}$, power available P_a, minimum autorotational inertia, and maximum allowable drag coefficient $c_{d_{all}}$ are 0.083 ft, 20 hp, 23.69 lbm-ft^2 and 0.12, respectively. Frequencies must be at least 0.1 away from a per rev value (Δf = 0.1 per rev in Eq. 6).

Study on the Effect of Initial Designs

The IADS multilevel decomposition optimization procedure is demonstrated for three examples using the three starting points shown in Fig. 8. Example 1 (Fig. 8a) uses a rectangular planform with a pretwist of -9.0 degrees, root chord of 0.3449 ft, and upper level stiffnesses design variables initialized to be consistent with the lower level initial wall thickness and lumped areas (i.e., matched stiffnesses). Example 2 (Fig. 8b) uses a tapered planform with a pretwist of -16.0 degrees, root chord of 0.45 ft, and matched stiffnesses. The blade is rectangular to 80 percent radius and then tapers linearly to the tip with a 3-to-1 taper ratio. Example 3 (Fig. 8c) uses the same planform and pretwist as Example 2 but the upper and lower level stiffnesses are not matched. All these examples use a value of -0.4 for the coordination parameter ε in Eq. 26. The importance of the choice of ε is examined in a later section of the paper.

Example 1 Rectangular Planform ("initially matched stiffnesses") - The starting point for the optimization is the rectangular blade shown in Fig. 8a. The upper and lower level stiffnesses are matched since the upper level stiffnesses are started with the stiffnesses determined by the initial lower level design variables. This is an infeasible starting point because the lower level stress constraints at the root are violated. Results are given in Table 3. The initial and final values for the blade planform, performance measures, and dynamics measures are given in the upper portion of Table 3. The initial and final values for the constrained frequencies are given in the middle portion of the table. Notice that the final value for the fourth bending frequency f_{b_4} is in a different frequency range than the initial value. Final values for the lower level design variables and the upper level stiffnesses are given in the bottom portion of the table. The final design is able to improve the performance characteristics from the initial blade and satisfy all the constraints. Compared to the initial values, the final design represents a 2.1, 2.3, 2.3, 47.6, and 3.2 percent reduction in the power required in hover, forward flight, and maneuver; hub shear; and upper level objective function, respectively.

The final stiffness distributions for the upper (required values) and lower levels (attainable values) are shown in Fig. 9. The matching of the chordwise bending stiffness EI_{xx} (Fig. 9a), the flapwise bending stiffness EI_{zz} (Fig. 9b), and the torsional stiffness GJ (Fig. 9c) are extremely good. As shown in Fig. 9d, the lower level is able to obtain an extensional stiffness distribution higher than the minimum requirement set by the upper level.

Convergence histories of the individual terms of the lower level objective function (Eq. 13) are shown in Fig. 10 for the three locations - the root (Fig. 10a), point of taper initiation (Fig. 10b), and the tip (Fig. 10c). Each term (denoted stiffness deviation) is a measure of how well the upper and lower stiffnesses match. Initially, the stiffnesses are matched, but the stress constraints are violated at the root. Therefore, the lower level design variables must change to satisfy these constraints while keeping the upper and lower level stiffnesses matched as close as possible. Notice that the chordwise stiffness at the root, torsional stiffness at the point of taper initiation, and flapwise stiffness at the tip are the last stiffnesses to match. Further, it appears that stiffnesses at the point of taper initiation are particularly difficult to match. This difficulty may be due to the fact that the point of taper initiation is a design variable while the root and tip positions are fixed.

The reason for the deviations in the stiffness is that the upper and lower levels are in conflict. One component of the upper level objective function is the hub shear which can be reduced significantly by increasing the blade stiffnesses. On the upper level if the optimizer did not have to be concerned with stiffness matching, it would increase the upper level stiffnesses. Without the lower level to keep the stiffnesses in check, a heavy or nonbuildable blade might result.

The information shown in Fig. 10 is collected and used to determine when an upper level design variable move limit adjustment is necessary during the overall optimization process (recall that approximate analysis is used on the upper level and exact analysis is used on the lower level). At the present time no automatic move limit adjustment in the approximate analysis on the upper level is used. Instead, the IADS procedure is run for eight cycles and then the stiffness deviations are examined. When the stiffness deviation increases (e.g. Cycle 16), the design variable move limits are manually reduced and the optimization process continued for another 8 cycles. In practical applications, the optimization procedure would terminate after about 30 cycles. However, for demonstration purposes the convergence criterion is set to a very small value. Both the upper and lower levels have the same tight convergence criterion on each cycle. Overall convergence of the IADS procedure might improve if the convergence criterion is relaxed initially and then tightened as the optimization proceeds.

Example 2 Tapered Planform ("initially matched stiffnesses") - The starting point for the optimization is the tapered blade shown in Fig. 8b. Initially, the upper and lower level stiffnesses are matched since the upper level stiffness are determined by the lower level design variables. However, this is an infeasible starting point since a thin wall theory constraint is violated on the lower level. The initial and final values for the blade planform, performance measures, and dynamics measures are given in Table 4. The final design is able to improve the performance characteristics from the initial blade. However, the hub shear increases from the initial value.

Fig. 11 shows the final stiffness distributions for the upper (required values) and lower levels (attainable values) for the chordwise bending stiffness (Fig. 11a), flapwise bending stiffness (Fig. 11b), and the torsional stiffness (Fig. 11c). As shown in the Fig., the stiffness matching is good, although not a good as in Example 1. The lower level is able to obtain an extensional stiffness distribution (Fig. 11d) higher than the minimum requirement.

Fig. 12 shows the stiffness deviations versus cycle for the three matching locations - the root (Fig. 12a), point of taper initiation (Fig. 12b), and the tip (Fig. 12c). Early in the optimization process, the flapwise and torsional stiffness are both unmatched. After Cycle 10, the matchings improve and after 25 cycles, all three matchings are good. At the tip (Fig. 12c) matching proves to be quite difficult. The torsional stiffness is the last to match. The reason for this is that the blade initial design is tapered and it is difficult to place a thin wall section in the space near and at the tip and still match the stiffness required on the upper level.

Example 3 Tapered planform ("initially unmatched stiffnesses") - In the previous examples, the starting points used matched stiffnesses. The purpose of this example is to demonstrate how the IADS procedure behaves when it is started from an inconsistent set of stiffnesses (i.e., unmatched stiffnesses). The starting point for the optimization is shown in Fig. 8c. The initial stiffnesses used in the upper level are much larger than the stiffnesses obtained from the lower level design variables. The initial and final values for the blade planform, performance measures, and dynamics measures are given in Table 5. The power required for all three flight conditions has increased substantially along with the hub shear. The initial and final constrained frequencies are also included. Notice that a bending frequency f_{b_6} has shifted frequency intervals.

The final upper and lower level stiffnesses are shown in Fig. 13. As shown in Fig. 13, the optimization procedure is able to match the upper and lower level stiffnesses successfully. Fig. 14 shows the stiffness deviations for the three matching locations - the root (Fig. 14a), the point of taper initiation (Fig. 14b), and the tip (Fig. 14c). As shown in the figure, after 25 cycles the optimization procedure is able to match all three stiffnesses, but it is at the expense of upper level performance (see Table 5). From these results it appears that while the optimization procedure will work when starting from an initial point which has unmatched stiffnesses, it is better to start with a set of consistent stiffnesses.

Observations on the Effect of Initial Design Study

The IADS procedure has been exercised for three starting blade planforms - a rectangular planform with matched stiffnesses, a tapered planform with matched stiffnesses, and a tapered blade with unmatched stiffnesses. In all cases the procedure is able to find converged feasible designs. Comparing Examples 1 and 2 (Tables 3 and 4, respectively), the reader will find two different final blade designs (i.e., design variable values are different) with essentially the same objective function value. Apparently, there are many different combinations of design variables which satisfy the matching conditions and more than one local minimum. The final solution depends on initial conditions. In Example 3 (Table 5), it appears that the optimizer converges to a suboptimal solution when compared with Example 2. Both examples started from the same planform, but Example 2 starts with matched stiffnesses and Example 3 starts with unmatched stiffnesses. Since the initial matching of the stiffnesses is relatively easy, this suggests that the initial matching should always be enforced.

Comparing all three examples, the reader will also notice that each initial blade has a different frequency range for the bending and torsional frequencies and each final blade design has a frequency which has shifted a frequency interval (e.g., f_{b_6} in Example 3). During the approximate analysis, the optimizer can change the upper level design variables such that a frequency can shift intervals. However, as the design variable move limits are reduced, this shifting is less likely to occur.

At the present time no automatic move limit adjustment in the upper level approximate analysis is used. However, the stiffness deviation information (e.g., Fig. 10) can be collected and used to determine when an upper level design variable move limit adjustment is necessary during the overall optimization process.

Study on the Effect of the Coordination Parameter ε

The purpose of this study is to demonstrate the effect of ε in the coordination constraint (Eq. 26) on the optimization procedure. Results for three ε values (+0.4, -0.2, and -0.4) are presented in Table 6 and Figs. 15-16, and 9, respectively. If ε is a large positive value, the levels are essentially independent. The upper level is free to change the upper level stiffness and chord distributions in any way which will reduce the upper level objective function. The only requirement is that the overall stiffness matching should not degrade by more than the amount ε from the best match found on the last lower level optimization. For example if ε is 0.4, the stiffness matching can degrade by 40 percent and still satisfy the coordination constraints. It is therefore possible that the procedure could converge with the upper and lower level stiffnesses being mismatched by as much as 40 percent. A negative value for ε means that the upper level must improve the matching achieved on the lower level by that amount. This section of the paper presents results for several values of ε using the starting point in Fig. 8a which is also used in Example 1.

One choice for ε would be zero. This would mean that the upper level cannot degrade the matching achieved on the lower level. This value was found to be too restrictive for the optimization process and the procedure converged in three cycles with very little change in the upper level design variables. The reason for this can be seen by examining the coordination constraint (Eq. 26). At the start of the upper level optimization, the coordination constraint at each matching location is active (i.e., g=0) since F^U is equal to F_o^L. As the upper level optimizer tries to change the upper level design variables, the coordination constraints become violated. Therefore, the upper level optimizer makes only small changes and the process converges in three cycles.

As shown in Table 6, when ε is 0.4, the optimization process is able to improve the performance and dynamics measures over the initial blade values and improve the lower level (satisfy the stress constraints). This improve-

ment is achieved at the expense of stiffness matching. Fig. 15 shows the final stiffness distributions for the upper and lower levels. The lower level is not able to find a set of stiffnesses to match those required by the upper level. This final result is technically a feasible design since all the constraints are satisfied. Recall the upper and lower stiffnesses need only be as close as possible (lower level objective function). The upper level coordination constraints do not require the upper and lower level stiffnesses to match exactly.

When ε is -0.2, the optimization procedure is able to obtain a design that has some improvement over the initial starting point (Table 6). The upper level objective function is reduced slightly, but not as much as when ε is positive. As shown in Fig. 16, the upper and lower stiffnesses match well for the chordwise stiffness (Fig. 16a), the flapwise stiffness (Fig. 16b), and the torsional stiffness (Fig. 16c). The lower level is able to obtain an extensional stiffness which is slightly larger than that required by the upper level.

Of the values used in this work, the best value for ε is -0.4. With this value of ε, the optimization procedure is able to obtain improvement on the upper level and find a set of consistent stiffnesses on the lower level. These results (Example 1) are included in Table 6 for completeness. The stiffness distributions are shown in Fig. 9.

As shown above, positive values of ε result in upper level improvement but poor stiffness matching and negative values of ε result in both upper level improvement (although not quite as good as when ε is positive) and good stiffness matching. This suggests that a gradual reduction from a positive to a negative value for ε could be beneficial. The IADS procedure was run with a value of +0.4 for ε for 8 cycles, +0.2 for 8 cycles, -0.2 for 8 cycles, and finally -0.4 for 8 cycles. This technique of gradually reducing the value of ε did not work. It is felt that the upper level planform area and upper level stiffnesses increased to improve the upper level objective function when ε was positive so that by the time ε was negative the stiffness matching was achieved at the expense of performance and dynamic improvement on the upper level. This situation is analogous to Example 3 where the mismatched initial conditions resulted in stiffness matching at the expense of upper level improvement.

Concluding Remarks

An integrated aerodynamic/dynamic/structural (IADS) optimization procedure for helicopter rotor blades has been developed. The procedure combines performance, dynamics, and structural analyses with a general purpose optimizer using multilevel decomposition techniques. At the upper level, the blade structure and response are represented in terms of global quantities (stiffnesses, mass, and average strains). At the lower level, the blade structure and response are represented in terms of local quantities (detailed dimensions and stresses).

The IADS procedure consists of an upper level optimization, a lower level optimization, and a coordination task. The upper level objective function is a linear combination of performance and dynamic measures. Upper level design variables include pretwist, point of taper initiation, taper ratio, root chord, blade stiffnesses, tuning masses, and tuning mass locations. Upper level constraints consist of limits on power required in hover, forward flight, and maneuver; airfoil drag; minimum tip chord; trim; blade natural frequencies; autorotational inertia; blade weight; and average strains.

The lower level optimization sizes the internal blade structure to provide the stiffnesses required by the upper level and assure the structural integrity of the blade. The lower level design variables are the box beam wall thicknesses and several lumped areas which are analogous to longitudinal stringers in a wing box cross section. The lower level objective function is a measure of the difference between the upper level stiffnesses and the stiffnesses computed from the wall thicknesses and lumped areas. The lower level constraints are on Von Mises stresses, extensional stiffnesses, thin wall theory, and dimensional limits.

The coordination task consists of a set of upper level constraints which link the levels and promote consistency between the upper and lower level stiffnesses. A coordination parameter is included in each constraint. This parameter specifies how much the upper level can degrade or must improve the overall stiffness matching achieved on the lower level and may also be interpreted as a measure of how closely-coupled the two levels are. It is found that a proper value for the coordination parameter is crucial to the success of the IADS procedure. If the parameter has a positive value, the procedure will converge but the final stiffness matching can be unacceptable. If the parameter has too small of a value (approximately zero), the optimization process will terminate without improving the dynamics or performance measures. A small negative value for the coordination parameter encourages the upper level to improve dynamics and performance using stiffness values which the lower level can match.

The IADS procedure is demonstrated using a model-size rotor blade for several initial blade planforms and varying amounts of coupling between the levels. In all cases, the IADS procedure achieves successful results. It converges to a feasible design regardless of whether or not the initial design had a set of consistent stiffnesses. However, initializing the upper level stiffnesses with the stiffnesses calculated from the lower level design variables, greatly improves the final design.

The IADS procedure exploits the couplings and interactions between the disciplines of aerodynamics, dynamics and structures. It provides an efficient method to integrate structures and/or structural properties into an optimization procedure since it guarantees that a structure with a consistent set of structural properties can be found. The IADS procedure provides an optimization technique that is compatible with industrial design practice in which the aerodynamic and dynamic design is performed at a global level and the structural design is carried out at a detailed level with considerable dialogue and compromise among the groups.

Appendix A - Coordination Constraint

In a multilevel decomposition approach, the coupling between levels is done through a coordination procedure (e.g. Refs. 20 and 25). In the present work, the coordination procedure based on Ref. 20 is used to reconcile the stiffnesses required on the upper level with the stiffnesses the lower level can actually obtain. This reconciliation results in one upper level constraint at each matching location

$$g = F^U - (1+\varepsilon)F_o^L \le 0 \tag{A1}$$

where F_o^L is the most recent value of the lower level objective function (i.e., optimum value of Eq. 13), F^U is an estimate of the change in F_o^L which would be caused by a change in the upper level design variable values, and ε is denoted the coordination parameter. This coordination parameter specifies how much the upper level can degrade or must improve the overall stiffness matching achieved on the lower level and may also be interpreted as a measure of how closely-coupled the two levels are. If ε has a positive value, the two levels are not closely-coupled (i.e., they are essentially independent). The upper level can change the upper level stiffness and chord distributions in any way which will improve the upper level objective function as long as the stiffness matching is not degraded by more than the amount ε. If ε has a negative value, the two levels are closely-coupled and the upper level is commanded to improve the matching by the amount ε.

Eq. A1 is the general form of the coordination constraint as formulated in Ref. 15. The form of the coordination constraint used in this work is obtained by approximating F^U in terms of the current optimum lower level objective function F_o^L. If F_o^L is expanded in terms of a first order Taylor series about the lower level optimum, then F^U can be approximated by

$$F^U = F_o^L + \sum_{i=1}^{NDV} \left.\frac{dF^L}{dDV_i}\right|_o \Delta DV_i \tag{A2}$$

where DV_i is an upper level design variable and $\left.\frac{dF^L}{dDV_i}\right|_o$ is the total optimum sensitivity derivative (Ref. 28) given by

$$\left.\frac{dF^L}{dDV_i}\right|_o = \left.\frac{\partial F^L}{\partial DV_i}\right|_o - \lambda^T \left.\frac{\partial KS}{\partial DV_i}\right|_o \tag{A3}$$

where $\frac{\partial F^L}{\partial DV_i}$ is the derivative of the optimum lower level objective function with respect to the upper level design variables, $\frac{\partial KS}{\partial DV_i}$ is the derivative of the active lower level constraint (Eq. 25) with respect to the upper level design variables, λ^T is the Lagrange multiplier given by

$$\lambda^T = -\left[\left(\frac{\partial KS}{\partial v}\right)^T \left(\frac{\partial KS}{\partial v}\right)\right]^{-1} \left.\frac{\partial F^L}{\partial v}\right|_0 \tag{A4}$$

where $\frac{\partial KS}{\partial v}$ is the derivative of the active lower level constraints with respect to the lower level design variables at the lower level optimum. At a lower level optimum, λ^T will be positive. If no lower level constraint is active, λ^T is set to zero. Substituting Eq. A2 into Eq. A1, the coordination constraint g is approximated by

$$g = \left[F_o^L + \sum_{i=1}^{NDV} \left.\frac{dF^L}{dDV_i}\right|_0 \Delta DV_i\right] - [1+\varepsilon]F_o^L \le 0 \tag{A5}$$

or simplifying

$$g = \left[\sum_{i=1}^{NDV} \left.\frac{dF^L}{dDV}\right|_0 \Delta DV\right] - \varepsilon F_o^L \le 0 \tag{A6}$$

Substituting Eq. A3 into Eq. A6, the coordination constraint becomes

$$g = \left\{\sum_{i=1}^{NDV}\left[\left.\frac{\partial F^L}{\partial DV_i}\right|_0 \Delta DV - \lambda^T \left.\frac{\partial KS}{\partial DV_i}\right|_0\right]\right\} - \varepsilon F_o^L \le 0 \tag{A7}$$

which is the form implemented in this work.

The derivative of the coordination constraint is obtained by differentiating Eq. A7 with respect to upper level design variables

$$\frac{\partial g}{\partial DV_i} = \left.\frac{\partial F^L}{\partial DV_i}\right|_0 \tag{A8}$$

Appendix B - Lower Level Structural Analysis

The purpose of this appendix is to summarize the elementary equations describing the geometry and structural analysis for the lower level structure. A typical cross section of the thin-walled isotropic box section is shown in Figure 5. For simplicity the top and bottom wall thicknesses, t_1 and t_3 are equal. The total cross-sectional area, A is the sum of the cross-sectional areas of the box beam elements A_i and the lumped areas a_j (described in the main text)

$$A = \sum_{i=1}^{n} A_i + \sum_{j=1}^{m} a_j \tag{B1}$$

Using the familiar relations, the centroid of the cross-section is calculated from the following equations

$$X_c = \frac{\sum_{i=1}^{n} A_i X_i + \sum_{j=1}^{m} a_j x_j}{A} \tag{B2}$$

and

$$Z_c = \frac{\sum_{i=1}^{n} A_i Z_i + \sum_{j=1}^{m} a_j z_j}{A} \tag{B3}$$

where X_i and Z_i are coordinates in the chordwise and flapwise directions respectively that specify the distance of the centroid of the ith element area A_i from the reference X and Z axes shown in Figure 5. Similarly, x_j and z_j are coordinates that specify the distance of the centroid of the jth lumped area a_j from the reference axes, n is the number of elements that the cross section is divided into for ease of calculations and m is the number of lumped areas.

Next, the area moments of inertia of each element about its centroidal X and Z axes are calculated from

$$I_{x_k} = \frac{b_k h_k^3}{12} \qquad k=1,...,n+m \tag{B4}$$

$$I_{z_k} = \frac{h_k b_k^3}{12} \qquad k=1,...,n+m \tag{B5}$$

where b_k is the base of the kth rectangular element and h_k is the height relative to the X axis and I_{xz_i} is equal to zero for symmetric elements. Using the parallel axis theorem, the moments of inertia of each element are found with respect to the centroid of the box beam as follows

$$\begin{aligned} I_{cx_k} &= I_{x_k} + A_k d_k^2 \\ I_{cz_k} &= I_{z_k} + A_k c_k^2 \end{aligned} \tag{B6}$$

where I_{cx_k}, and I_{cz_k} are the moments of inertia of the kth element about the centroid of the box beam, I_{x_k} and I_{z_k} are the moments of inertia of the kth element about its centroidal axes, d_k and c_k are the distances from the centroid of the element to the centroid of the box beam in the X and Z directions respectively. The total moments of inertia for the box beam are equal to the sum of the element inertias.

$$\begin{aligned} I_{xx} &= \sum I_{cx_k} \\ I_{zz} &= \sum I_{cz_k} \end{aligned} \tag{B7}$$

The polar moment of inertia for the box beam is calculated using the method described in Ref. 38.

$$J = \frac{4A_c^2}{\oint ds / t} \tag{B8}$$

where A_c is the enclosed area of the mean periphery of the box beam wall, ds is the differential circumferencial length along the box beam, and t is the local thickness of the wall.

In order to calculate the lower level objective function, the bending and torsional stiffnesses of the box beam are necessary. For an isotropic beam the moments of inertia, I_{xx} and I_{zz}, calculated above are multiplied by Young's Modulus E to acquire the bending stiffnesses, EI_{xx} and EI_{zz}, in the chordwise and flapwise directions respectively. Similarly, the polar moment of inertia is multiplied by the torsional modulus of elasticity G to acquire the torsional stiffness of the beam, GJ.

The stresses for the constraints in the lower level optimization are evaluated at the corners of the box beam using Von Mises stress measure which is given by

$$V(\sigma,\tau) = \sqrt{\sigma^2 + 3\tau^2} \quad \text{(B9)}$$

where σ is the axial bending stress at the outer fiber of the cross section

$$\sigma = \left(\frac{M_{zz}}{I_{zz}}\right) X_{outer} + \left(\frac{M_{xx}}{I_{xx}}\right) Z_{outer} + \frac{CF}{A} \quad \text{(B10)}$$

and τ is the shear stress due to torsion in the wall of the section with thickness t

$$\tau = \frac{M_T}{2A_c t} \quad \text{(B11)}$$

where M_{zz} is the flapwise moment; M_{xx} is the lag moment; CF is the centrifugal force; and M_T is the torque at the section. The shear stress due to transverse loads has been neglected for simplicity. M_{zz}, M_{xx}, CF, and M_T are computed in the upper level analysis for forward flight and maneuver, multiplied by a factor of safety l_f, and then passed to the lower level.

References

1. Miura, H.: Applications of Numerical Optimization Methods to Helicopter Design Problems: A Survey. NASA TM-86010, October 1984.

2. Bennett, R. L.: Application of Optimization Methods to Rotor Design Problems. Vertica, Vol. 7, No. 3, 1983, pp. 201-208.

3. Walsh, J. L.; Bingham, G. J.; and Riley, M. F.: Optimization Methods Applied to the Aerodynamic Design of Helicopter Rotor Blades. Journal of the American Helicopter Society, Vol 32, No. 4, October 1987.

4. Walsh, J. L.: Performance Optimization of Helicopter Rotor Blades. NASA TM-104054, April 1991.

5. Nixon, M. W.: Preliminary Structural Design of Composite Main Rotor Blades for Minimum Weight. NASA TP-2730, July 1987.

6. Friedmann, P. P. and Shantakumaran, P.: Optimum Design of Rotor Blades for Vibration Reduction in Forward Flight. Proc. of the 39th Annual Forum of the AHS, May 9-11, 1983, St. Louis, Missouri.

7. Peters, D. A.; Ko, T,; Korn, A.; and Rossow, M. P.: Design of Helicopter Rotor Blades for Desired Placements of Natural Frequencies. Proceedings of the 39th Annual Forum of the AHS. May 9-11, 1983, St. Louis, Missouri..

8. Davis M. W. and Weller, W. H.: Application of Design Optimization Techniques to Rotor Dynamics Problems. Journal of the American Helicopter Society, Vol 33, No. 3, July 1988.

9. Celi, R. and Friedmann, P. P.: Efficient Structural Optimization of Rotor Blades with Straight and Swept Tips. Proc. of the 13th European Rotorcraft Forum, Arles, France, September 1987. Paper No. 3-1.

10. Friedmann, P. P.: Impact of Structural Optimization with Aeroelastic/Multidisciplinary Constraints on Helicopter Rotor Design. AIAA Paper No. 92-1001, Presented at 1992 Aerospace Design Conference. Irvine, California, February 3-6, 1992.

11. Adelman, H. M. and Mantay, W. R.: Integrated Multidisciplinary Optimization of Rotorcraft: A Plan of for Development. NASA TM-101617 (AVSCOM TM 89-B-004). May 1989.

12. Adelman, H. M. and Mantay, W. R.: Integrated Multidisciplinary Optimization of Rotorcraft. Journal of Aircraft, Vol. 28, No. 1, January 1991.

13. Chattopadhyay, A.; Walsh J. L.; and Riley, M. F.: Integrated Aerodynamic Load/Dynamic Optimization of Helicopter Rotor Blades. Journal of Aircraft, Vol. 28, No. 1, January 1991.

14. Walsh, J. L.; LaMarsh, W. J.; and Adelman, H. M.: Fully Integrated Aerodynamic/Dynamic Optimization of Helicopter Rotor Blades. NASA TM-104226, February 1992.

15. Adelman, H. M.; Walsh, J. L.; and Pritchard, J. I.: Recent Advances in Integrated Multidisciplinary Optimization of Rotorcraft. Proceedings of the Fourth AIAA/USAF/NASA/OAI Symposium on Multidisciplinary Analysis and Optimization. Cleveland, Ohio, September 21-23, l992. Also available as NASA TM-107665 (AVSCOM TM 92-B-012) September 1992.

16. Straub, F. K.; Callahan, C. B.; and Culp, J. D.: Rotor Design Optimization Using a Multidisciplinary Approach. AIAA Paper No. 91-0477, Presented as the 29th Aerospace Sciences Meeting. Reno, Nevada, January 7-10, 1991.

17. Callahan, C. B. and Straub, F. K.: Design Optimization of Rotor blades for Improved Performance and Vibrations. Proceedings of the 47th Annual Forum of the American Helicopter Society. Phoenix, Arizona, May 6-8, 1991.

18. He, C. and Peters, D. A.: Optimization of Rotor Blades for Combined Structural, Dynamic, and Aerodynamic Properties. Structural Optimization, 5, pp 37-44, 1992.

19. Chattopadhyay, A.; and Narayan, J. R.: Optimum Design of High Speed Prop-rotors Using a Multidisciplinary Approach. Proceedings of the 48th Annual Forum of the American Helicopter Society. Washington, D.C., June 3-5, 1992.

20. Sobieszczanski-Sobieski, J.: Two Alternative Ways for Solving the Coordination Problem in Multilevel Optimization. NASA TM-104036, August 1991.

21. Chattopadhyay, A.; McCarthy, T. R.; and Padaldipti, N.: A Multilevel Decomposition Procedure for Efficient Design Optimization of Helicopter Rotor Blades. Presented at the 19th European Rotorcraft Forum, Cernobbio, Italy, September 14-16, 1993. Paper No. G7.

22. Sobieszczanski-Sobieski, J; James, B. B.; and Dovi, A. R.: Structural Optimization by Multilevel Decomposition. AIAA J., Vol. 23, No. 11, November l985, pp. 1775-1782.

23. Wrenn G. A. ; and Dovi, A. R.: Multilevel Decomposition Approach to the Preliminary Sizing of a Transport Aircraft Wing. AIAA Journal of Aircraft, Vol. 25, No. 7, July 1988, pp 632-638.

24. Zeiler, T. A.; and Gilbert, M. G.: Integrated Control/Structure Optimization by Multilevel Decomposition. AIAA Paper No. 90-1057. Presented at AIAA/ASME/ASCE/AHS/ASC 31st Structures, Structural Dynamics and Materials Conference. Long Beach, California, April 2-4, 1990.

25. Sobieszczanski-Sobieski, J.: A Linear Decomposition Method for Large Optimization Problems--Blueprint for Development. NASA TM-83248, February 1982.

26. Sobieszczanski-Sobieski, J.,: Barthelemy, J. F.; Riley, K. M.: Sensitivity of Optimum Solutions to Problem Parameters. AIAA J., Vol. 21, Sept. 1982, pp. 1291-1299.

27. Thareja, R.; and Haftka, R. T.: Numerical Difficulties Associated with Using Equality Constraints to Achieve Multi-level Decomposition in Structural Optimization. AIAA Paper No. 86-0854. AIAA/ASME/ASCE/AHS 27th Structures, Structural Dynamics, and Materials Conference. San Antonio, Texas. May 1986.

28. Barthelemy, J. F.; and Sobieszczanski-Sobieski, J.: Optimum Sensitivity Derivatives of Objective Functions in Nonlinear Programing. AIAA J., Vol. 22, June 1983, pp. 913-915.

29. Kresselmeir, G.; and Steinhauser, G.: Systematic Control Design by Optimizing a Vector Performance Index. Proceedings of IEAC Symposium on Computer Aided Design of Control Systems. Zurich, Switzerland, l971.

30. Gessow, A.; and Myers, G. C., Jr.: Aerodynamics of the Helicopters. Frederick Unger Publishing Company, New York, 1952.

31. Johnson, W.: CAMRAD/JA - A Comprehensive Analytical Model of Rotorcraft Aerodynamics and Dynamics - Johnson Aeronautics Version. Volume I: Theory Manual and Volume II: User's Manual. Johnson Aeronautics, 1988.

32. Rosenstein, H.; and Clark, R.: Aerodynamic Development of the V-22 Tilt Rotor. Paper No. 14. Twelfth European Rotorcraft Forum. Gramisch-Partenkirchen, Germany. Setpember 22-25, l986.

33. Vanderplaats, G. N.: CONMIN - A Fortran Program for Constrained Function Minimization. User's Manual. NASA TMX-62282. August 1973.

34. Walsh, J. L.: Computer-aided Design of Light Aircraft to Meet Certain Aerodynamic and Structural Requirements. Master's Thesis. Old Dominion University. August 1973.

35. Noonan, K. W.: Aerodynamic Characteristics of Two Rotorcraft Airfoils Designed for Application to the Inboard Region of a Main Rotor Blade. NASA TP-3009, AVSCOM TR-90-B-005. July 1990.

36. Bingham, G. J.; and Noonan, K. W.: Two-Dimensional Aerodynamic Characteristics of Three Rotorcraft Airfoils at Mach Numbers From 0.35 to 0.90. NASA TP-2000, AVRADCOM TR-82_B-2. May 1982.

37. Wilbur, M. L.: Experimetnal Investigation of Helicopter Vibration Reduction Using Rotor Blade Aeroelastic Tailoring. Proceedings of the 47th Annual Forum of the American Helicopter Society. Phoenix, Arizona, May 6-8, 1991.

38. Bruhn, E. F.: Analysis and Design of Flight Vehicle Structures, Tri-state Offset Co. Cincinnati, Ohio.

Table 1. Design variable bounds

	Design variables Lower bound	Upper bound
Twist (deg)	–20.0	–5.0
Point of taper initiation (r/R)	0.26	0.985
Taper ratio	0.05	5.0
Root chord (ft)	0.05	0.833
EI_{xx} (lbm-ft^2)	50.00	20000000.0
EI_{zz} (lbm-ft^2)	5.00	1000.0
GJ (lbm-ft^2)	5.00	1000.0
EA (lbm)	1000.00	200000000.0
m_i (slug/ft)	0.0	0.50
y_i (r/R)	0.24	0.95
t_i (ft)	0.00008	0.01
a_i (ft^2)	0.0	0.00004

Table 2. Parameters and flight conditions

Parameters	
Minimum autorotational inertia, AI_{min}	23.69 lbm-ft^2
Allowable drag coefficient, $c_{d_{all}}$	0.12
Minimum tip chord, $c_{t_{min}}$	0.083 ft
Number of blades, N	4
Number of aerodynamic segments	
HOVT	19
CAMRAD/JA	18
Number of structural segments	50
Number of design variables	
Upper level	22
Lower level	18 (6 per location)
Power available, P_a	20 hp
Blade radius, R	4.68 ft
Maximum blade mass, W	3.5 lbm
Factor of safety, l_f	2.0
Δf	0.1 per rev
Allowable average strain, ε_a	0.05 ft/ft
$ITER_{max}$	40
ρ_{max}	300
Allowable stress, σ_a	8.352x10^6 b/ft^2
Young's modulus, E	15.26x10^8 lb/ft^2

Flight conditions			
Rotational velocity	639.5 RPM (in Freon density of 0.006 slug/ft^3)		
Hover tip Mach number	0.628		
	Hover	Forward flight	Maneuver
C_L	0.00810	0.00810	0.00985
C_D	–	–0.000811	–0.000596
Advance ratio	–	0.35	0.30

Table 3 - Rectangular planform starting point with matched stiffnesses - Example 1

	Initial	Final
Hover power (hp)	14.81	14.50
Forward flight power (hp)	13.26	12.96
Maneuver power (hp)	12.22	11.94
Hub shear (lb)	2.1	1.1
Objective function	20.58	19.91
Twist (deg)	-9.0	-11.47
Taper initiation	0.7	0.701
Taper ratio	1.0	1.66
Root chord(ft)	0.3449	0.3770
m_1 (slug/ft)	0.0	0.0002761
m_2 (slug/ft)	0.0	0.003199
m_3 (slug/ft)	0.0	0.002014
y_1 (ft)	-	0.450
y_2 (ft)	-	0.583
y_3 (ft)	-	0.0453
Cycles to converge	-	76
f_{b_3} per rev	2.60	2.68
f_{b_4} per rev	3.77	4.57
f_{b_5} per rev	4.52	4.88
f_{b_6} per rev	7.22	7.55
f_{t_1} per rev	7.30	7.30
f_{t_2} per rev	3.61	3.83

Final Design Variables	Root	Point of taper initiation	Tip
Lower Level			
t_1 (ft)	0.002366	0.002427	0.0004517
t_2 (ft)	0.003261	0.009954	0.0003766
t_4 (ft)	0.003414	0.009954	0.0003766
a_1 (ft^2)	0.00003341	0.00003293	0.00001610
a_2 (ft^2)	0.00001615	0.00003084	0.00001192
a_3 (ft^2)	0.00003281	0.00003293	0.00001610
Upper Level			
EI_{xx} (lb-ft^2)	2057.0	2974.1	153.7
EI_{zz} (lb-ft^2)	122.21	140.03	8.61
GJ (lb-ft^2)	127.93	128.53	5.87
EA (lb)	797370.	1647300.	212230.

Table 4 - Tapered planform starting point with matched stiffnesses - Example 2

	Initial	Final
Hover power (hp)	14.85	14.74
Forward Flight power (hp)	13.38	13.02
Maneuver power (hp)	11.93	11.84
Hub shear (lb)	0.6	0.66
Objective function	19.88	19.93
Twist (deg)	-16.0	-10.85
Point of taper initiation	0.8	0.37
Taper ratio	3.0	1.64
Root chord (ft)	0.45	0.4932
m_1 (slug/ft)	0.0	0.008961
m_2 (slug/ft)	0.0	0.01354
m_3 (slug/ft)	0.0	0.0246
y_1 (ft)	-	0.24
y_2 (ft)	-	0.616
y_3 (ft)	-	0.622
Cycles to converge	-	93
f_{b_3} per rev	2.93	2.86
f_{b_4} per rev	5.64	5.33
f_{b_5} per rev	6.22	6.68
f_{b_6} per rev	10.25	9.16
f_{t_1} per rev	7.30	7.30
f_{t_2} per rev	6.45	6.12

Table 5 - Tapered planform starting point with unmatched stiffnesses - Example 3

	Initial	Final
Hover power (hp)	14.85	16.64
Forward flight power (hp)	13.27	17.46
Maneuver power (hp)	11.89	14.89
Hub shear (lb)	0.186	2.45
Objective Function	20.01	24.62
Twist (deg)	-16.0	-11.98
Point of taper initiation	0.8	.889
Taper ratio	3.0	1.3148
Root chord (ft)	0.45	0.7364
m_1 (slug/ft)	-	0.008546
m_2 (slug/ft)	-	0.007797
m_3 (slug/ft)	-	0.009030
y_1 (ft)	-	0.323
y_2 (ft)	-	0.439
y_3 (ft)	-	0.393
Cycles to converge	-	92
f_{b_3} per rev	2.87	2.90
f_{b_4} per rev	5.54	5.87
f_{b_5} per rev	8.62	8.10
f_{b_6} per rev	9.65	10.5
f_{t_1} per rev	7.30	7.30
f_{t_2} per rev	5.48	5.12

Table 6- Effect of ε on multilevel decompostion optimization procedure

	Initial	Final	Final	Final
ε		+.4	-.2	-.4
Hover power (hp)	14.81	14.44	14.60	14.50
Forward flight power (hp)	13.26	12.77	13.11	12.96
Maneuver power (hp)	12.22	11.75	11.96	11.94
Hub shear (lb)	2.1	0.2072	1.85	1.1
Objective function	20.58	19.48	20.22	19.91
Twist (deg)	-9.0	-13.32	-11.12	-11.47
Point of taper initiation	0.7	0.786	0.825	.701
Taper ratio	1.0	3.16	1.41	1.66
Root chord (ft)	0.3449	0.3651	0.3606	0.3770
m_1 (slug/ft)	0.0	0.02571	0.00135	0.0002761
m_2 (slug/ft)	0.0	0.00211	0.0000995	0.003199
m_3 (slug/ft)	0.0	0.00099	0.0000727	0.002014
y_1 (ft)	-	0.4124	0.3115	0.450
y_2 (ft)	-	0.4154	0.3950	0.583
y_3 (ft)	-	0.4382	0.4292	0.453
Cycles to converge	-	90	152	76

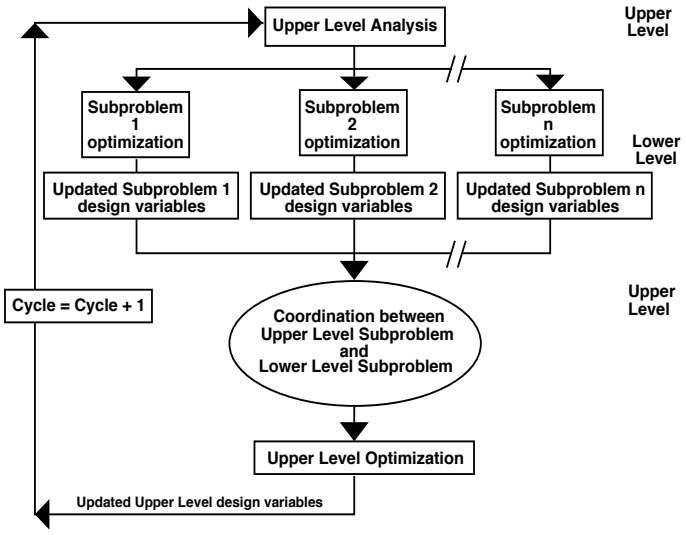

Figure 1. General multilevel optimization procedure with two levels.

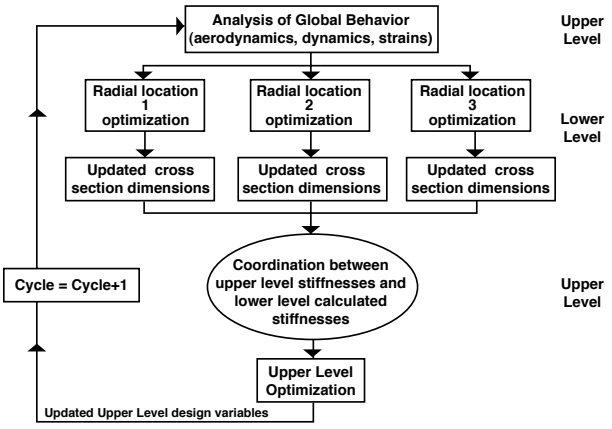

Figure 2. Multilevel strategy for rotor blade aerodynamic, dynamic and structural optimization

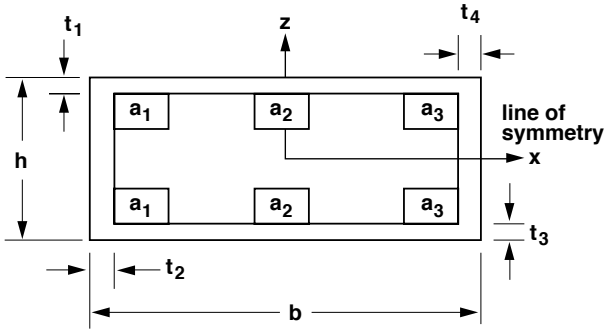

Figure 5. Lower level design variables

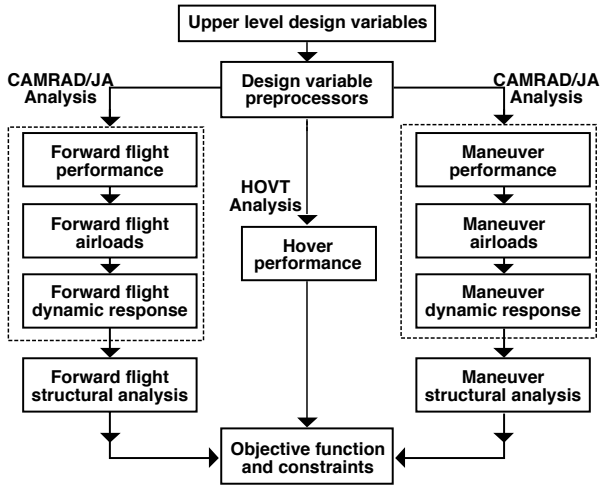

Figure 3. Upper level analysis flowchart

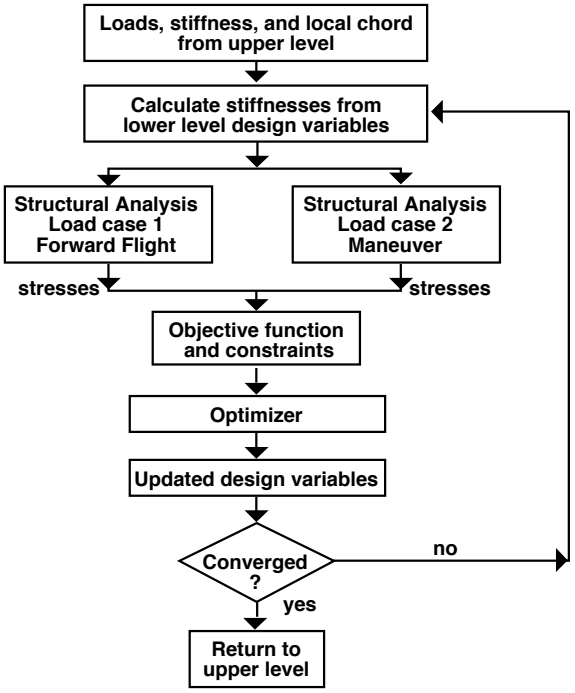

Figure 6. Lower level flowchart

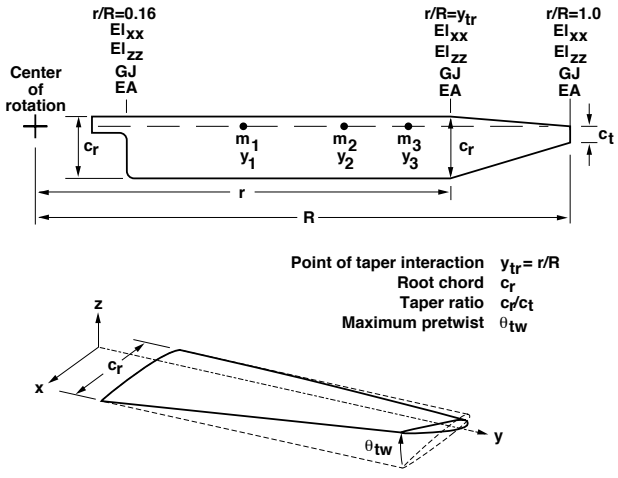

Figure 4. Upper level design variables

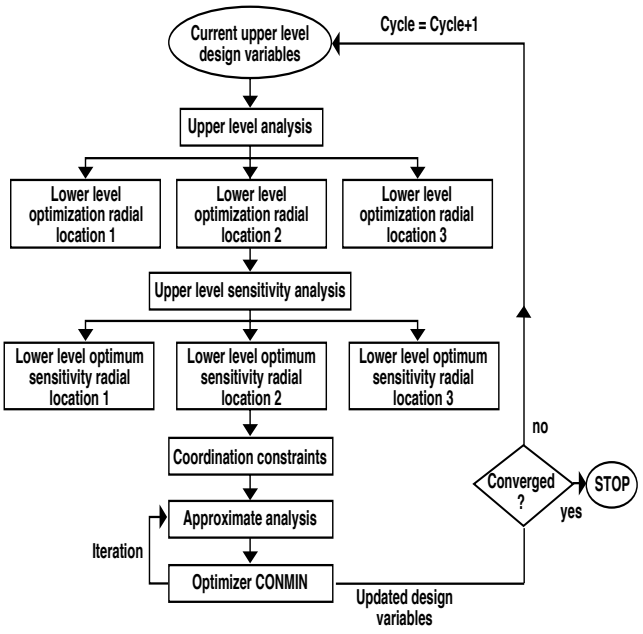

Figure 7. Overall optimization flowchart

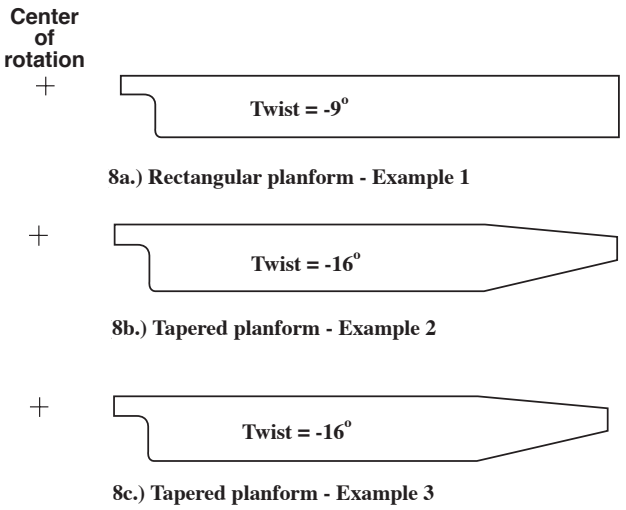

Figure 8. Initial designs used to start IADS procedure

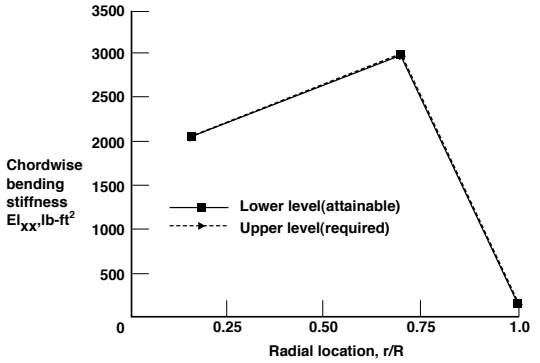

9a) Chordwise bending stiffness

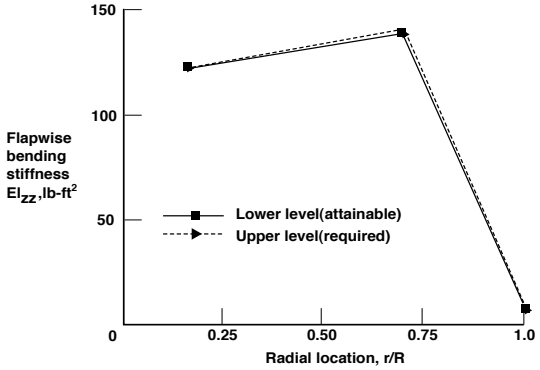

9b) Flapwise bending stiffness

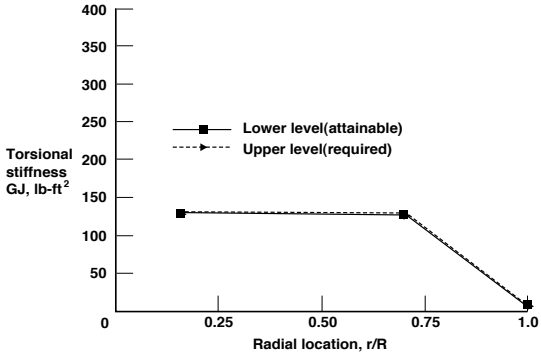

9c) Torsional stiffness

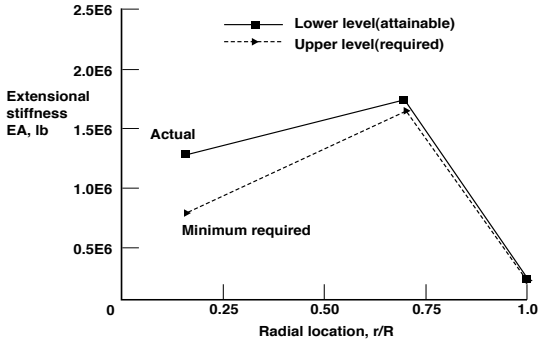

9d) Extensional stiffness

Figure 9. Final upper and lower level stiffness distributions - Example 1

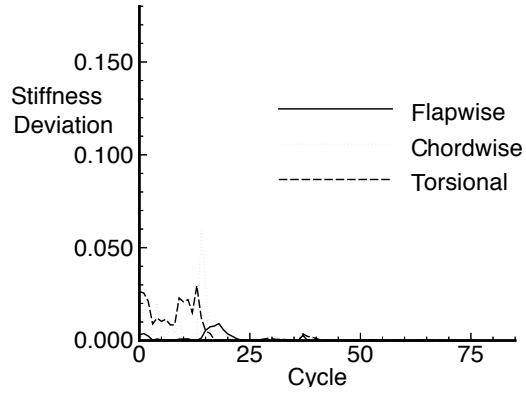

10a) Root

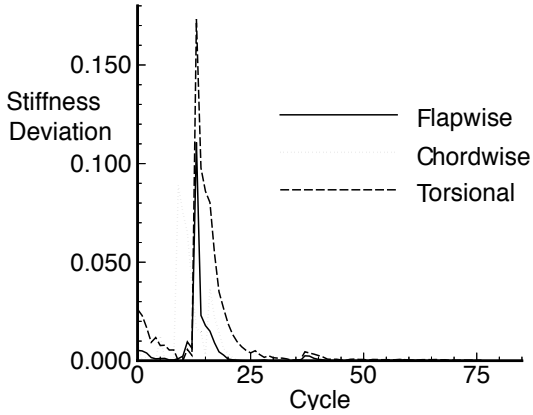

10b) Point of taper initiation

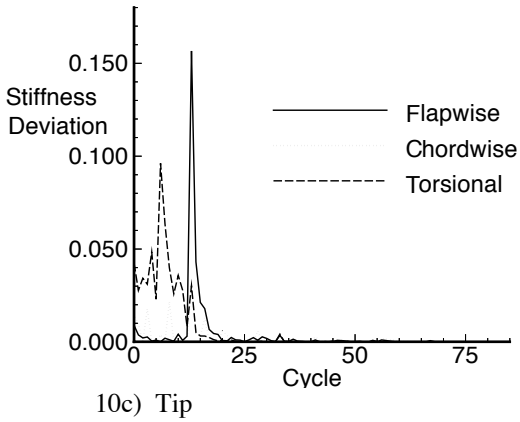

10c) Tip

Figure 10. Convergence history of upper and lower level stiffness deviations - Example 1.

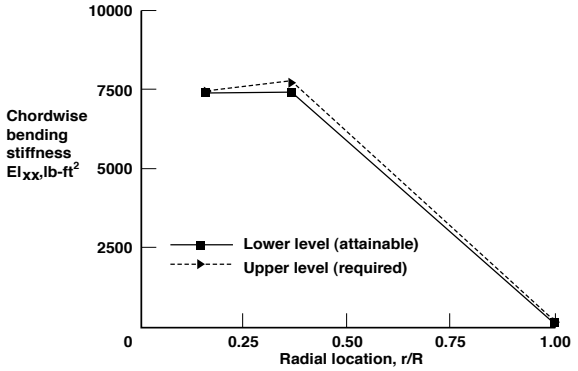

11a) Chordwise bending stiffness

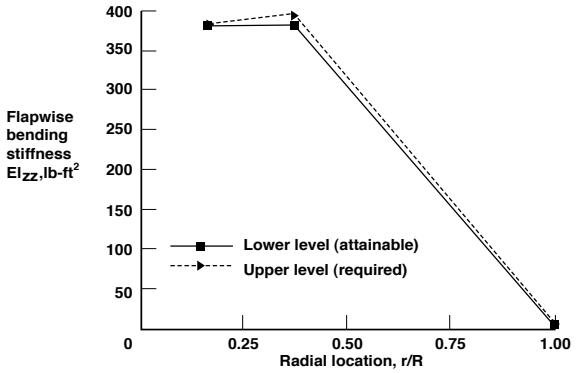

11b) Flapwise bending stiffness

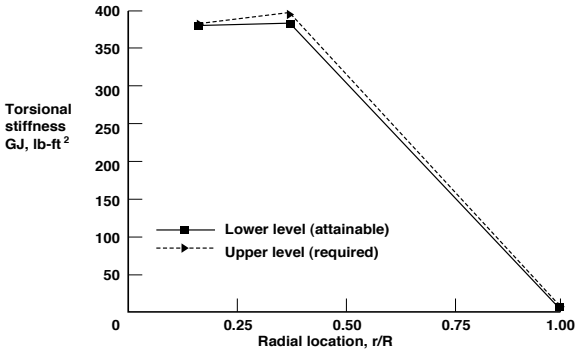

11c) Torsional stiffness

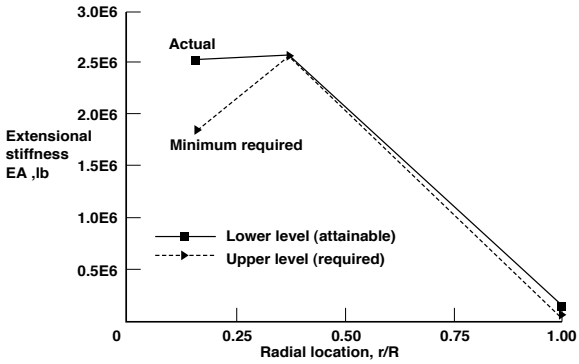

11d) Extensional stiffness

Figure 11. Final upper and lower level stiffness distributions - Example 2

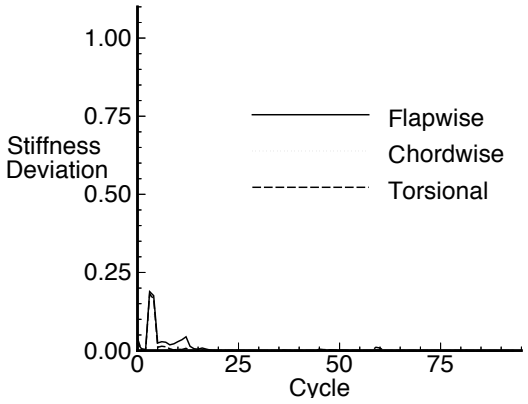

12a) Root

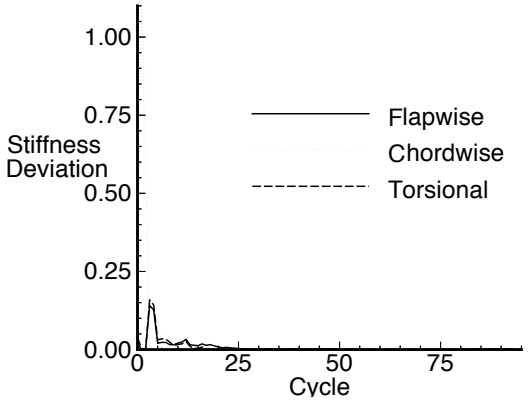

12b) Point of taper initiation

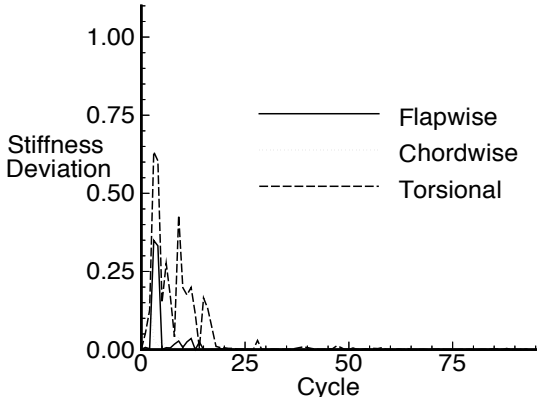

12c) Tip

Figure 12. Convergence history of upper and lower level stiffness deviations - Example 2.

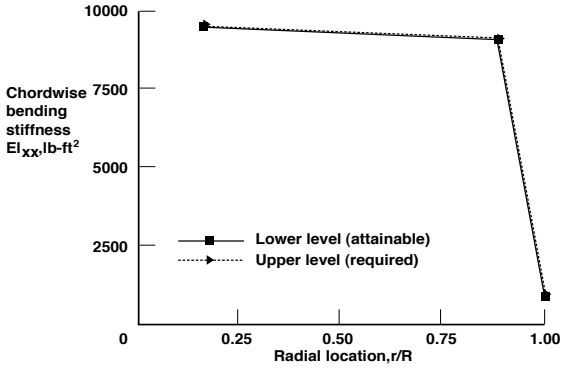

13a) Chordwise bending stiffness

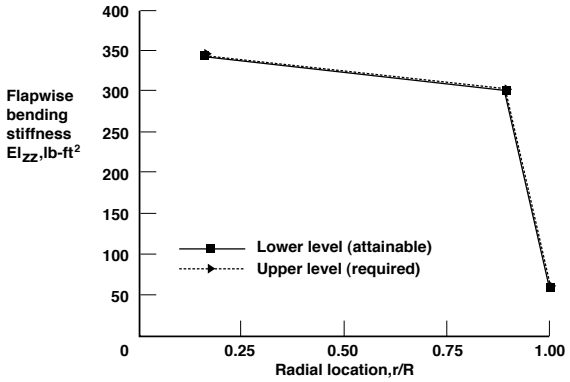

13b) Flapwise bending stiffness

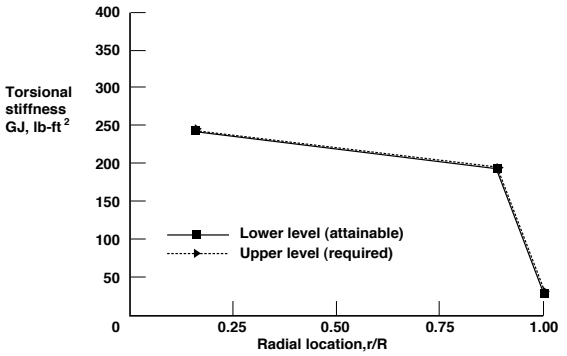

13c) Torsional stiffness

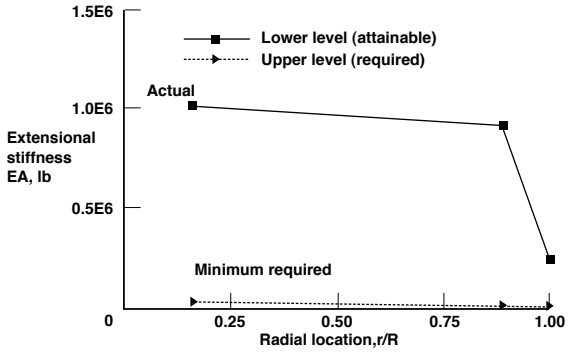

13d) Extensional stiffness

Figure 13. Final upper and lower level stiffness distributions - Example 3

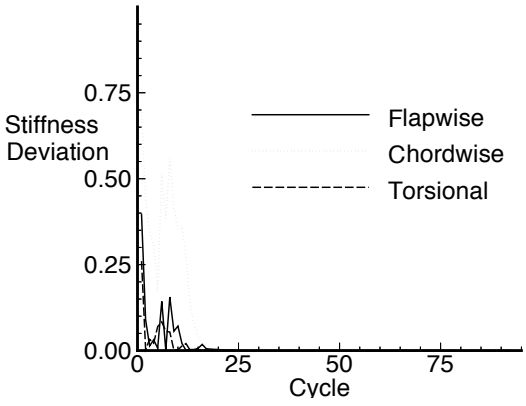

14) Root

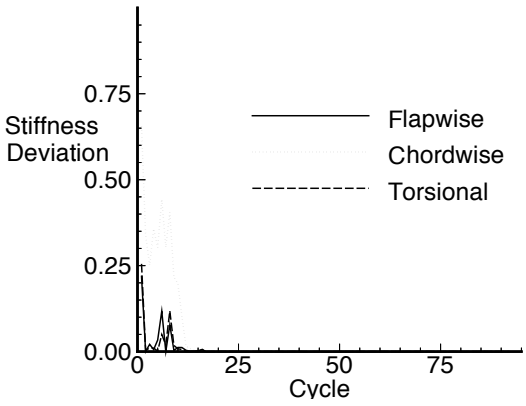

14b) Point of taper initiation

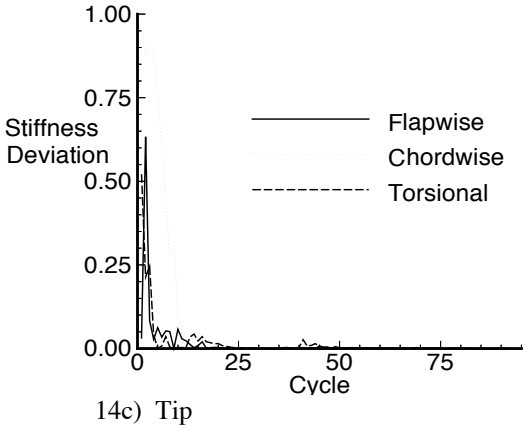

14c) Tip

Figure 14. Convergence history of upper and lower level stiffness deviations - Example 3.

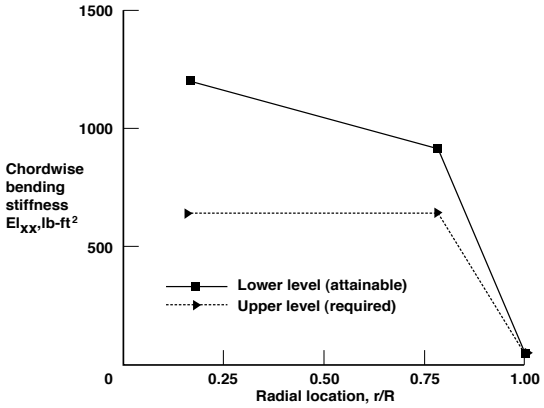

15a) Chordwise bending stiffness

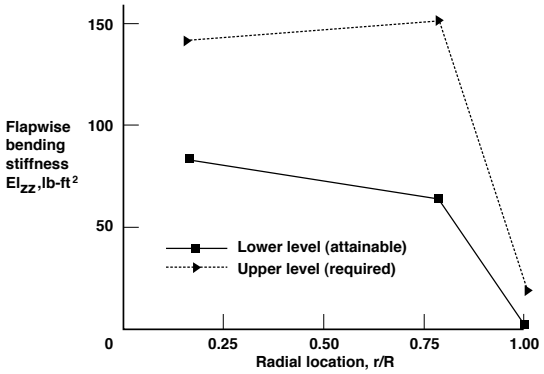

15b) Flapwise bending stiffness

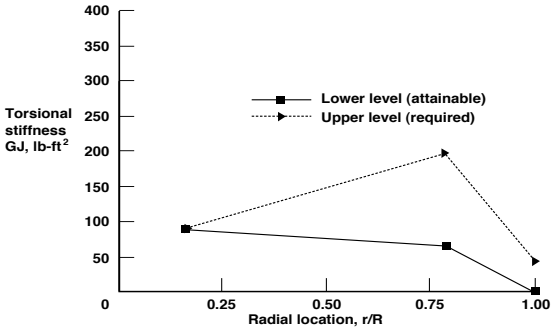

15c) Torsional stiffness

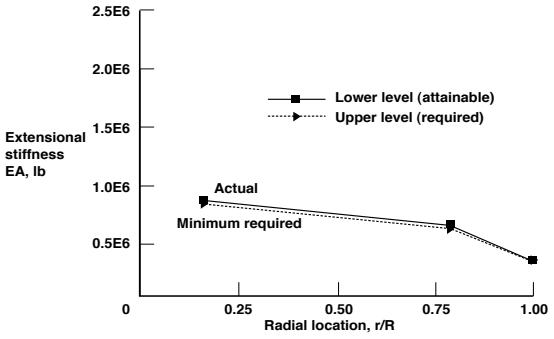

15d) Extensional stiffness

Figure 15. Final upper and lower level stiffness distributions for ε=+0.4

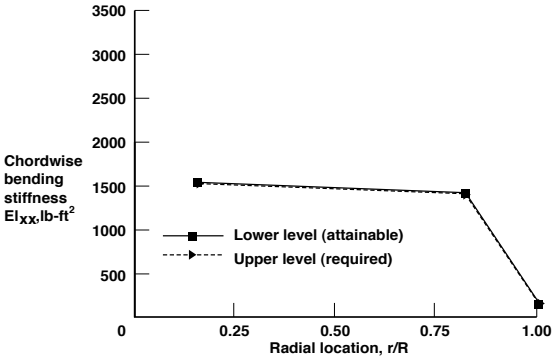

16a) Chordwise bending stiffness

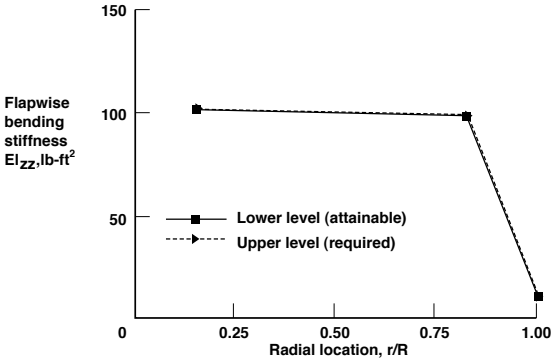

16b) Flapwise bending stiffness

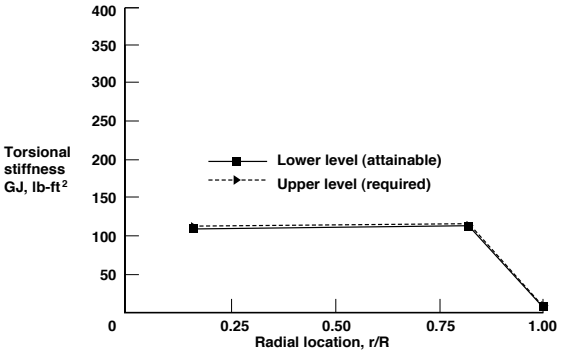

16c) Torsional stiffness

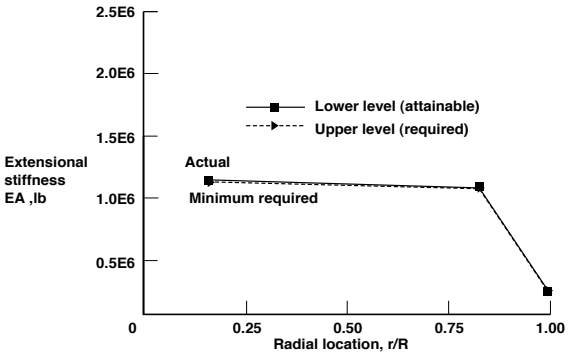

16d) Extensional stiffness

Figure 16. Final upper and lower level stiffness distributions for ε=-0.2